ISTANBUL TECHNICAL UNIVERSITY ★ GRADUATE SCHOOL

MULTI-OBJECTIVE OPTIMIZATION OF FIBER REINFORCED LAMINATED HYBRID COMPOSITE PLATES USING PARTICLE SWARM ALGORITHM

M.Sc. THESIS

Orhan Nuri YEGIT

Department of Aeronautics and Astronautics Engineering

Aeronautics and Astronautics Engineering Programme

JULY 2024

ISTANBUL TECHNICAL UNIVERSITY ★ GRADUATE SCHOOL

MULTI-OBJECTIVE OPTIMIZATION OF FIBER REINFORCED LAMINATED HYBRID COMPOSITE PLATES USING PARTICLE SWARM ALGORITHM

M.Sc. THESIS

Orhan Nuri YEGIT
(511201178)

Department of Aeronautics and Astronautics Engineering

Aeronautics and Astronautics Engineering Programme

Thesis Advisor: Asst. Prof. Kaan YILDIZ

JULY 2024

İSTANBUL TEKNİK ÜNİVERSİTESİ ★ LİSANSÜSTÜ EĞİTİM ENSTİTÜSÜ

FİBER TAKVİYELİ KATMANLI HİBRİT KOMPOZİT PLAKALARIN PARÇACIK SÜRÜ ALGORİTMASI İLE ÇOK AMAÇLI OPTİMİZASYONU

YÜKSEK LİSANS TEZİ

Orhan Nuri YEGIT
(511201178)

Uçak ve Uzay Mühendisliği Anabilim Dalı

Uçak ve Uzay Mühendisliği Programı

Tez Danışmanı: Dr. Öğr. Üyesi Kaan YILDIZ

TEMMUZ 2024

Orhan Nuri YEGIT, a M.Sc. student of ITU Graduate School student ID 511201178 successfully defended the thesis entitled “MULTI-OBJECTIVE OPTIMIZATION OF FIBER REINFORCED LAMINATED HYBRID COMPOSITE PLATES USING PARTICLE SWARM ALGORITHM”, which he prepared after fulfilling the requirements specified in the associated legislations, before the jury whose signatures are below.

Thesis Advisor :	**Asst. Prof. Kaan YILDIZ** Istanbul Technical University	....
Jury Members :	**Prof. Dr. Aytaç ARIKOĞLU** Istanbul Technical University	....
	Asst. Prof. Fatih USTA Gebze Technical University	....

Date of Submission : **22 May 2024**
Date of Defense : **02 July 2024**

To my family,

FOREWORD

I am excited to share this thesis, which represents years of hard work and learning. I would like to express my deepest gratitude to my advisor Asst. Prof. Kaan Yıldız for their encouragement, guidance and endless support throughout this study.

I would like to state that I am grateful to my family, especially my parents, Nurcan Yegit and Behçet Yegit who supporting and believing me under all circumstances. I always feel your support behind me.

I want to thank my friends and colleagues at Turkish Aerospace Ind. for their support and friendship. Studying together and sharing ideas has made my academic journey even better. I would also like to thank my company for its support during my master's program.

July 2024 Orhan Nuri YEGIT

TABLE OF CONTENTS

ABBREVIATIONS

ACO	: Ant Colony Optimization
CLT	: Classical Lamination Theory
CPT	: Classical Plate Theory
DE	: Differential Evaluation Algorithm
GA	: Genetic Algorithm
PSO	: Particle Swarm Optimization
SA	: Simulated Annealing

SYMBOLS

A_{ij}	: Plate's extensional stiffness matrix
a	: Plate length
B_{ij}	: Plate's bending-extension coupling stiffness matrix
b	: Plate width
c	: $\cos\theta$
c_1	: Personal acceleration factor
c_2	: Global acceleration factor
D_{ij}	: Plate's bending stiffness matrix
E	: Young modulus
G	: Shear modulus
h	: The total thickness of the plate
K_c	: The number of carbon fiber in the laminate
K_g	: The number of glass fiber in the laminate
M_x, M_y, M_{xy}	: The in-plane moment resultants
m	: Half-wave numbers in the x direction
N_x, N_y, N_{xy}	: The in-plane stress resultants
n	: Half-wave numbers in the y direction
Q	: Lamina stiffness matrix
Q_x, Q_y	: Transverse shear forces
$\overline{Q}$	: Reduced stiffness matrix
r	: Aspect ratio
r_p	: Penalty function coefficient
SSSS	: Simply supported on all sides of plates
s	: $\sin\theta$
T	: Transformation matrix
t	: The layer thickness
w	: Vertical displacement
α_0	: Cost ratio
γ_{xy}^0	: The mid-plane strains
$\varepsilon_x^0, \varepsilon_y^0$	: The mid-plane strains
θ	: Fiber orientation
$\kappa_x, \kappa_y, \kappa_{xy}$	: Curvature of the plane
λ_b	: Buckling factor
$\lambda_{c,b}$	: Critical buckling factor
ν	: Poisson's ratio
ρ	: Density
ρ_c	: The density of the carbon fiber
ρ_g	: The density of the glass fiber
σ_x, σ_y	: The in-plane normal stress
τ_{xy}	: The in-plane normal stress

LIST OF TABLES

Page

LIST OF FIGURES

Page

MULTI-OBJECTIVE OPTIMIZATION OF FIBER REINFORCED LAMINATED HYBRID COMPOSITE PLATES USING PARTICLE SWARM ALGORITHM

SUMMARY

This study investigates the multi-objective optimization of layered hybrid composite structures under axial compressive loads using the particle swarm optimization (PSO) approach. A simply supported composite plate consisting of 64 layers was subjected to constant axial compressive loads in two directions. The classical plate theory (Kirchoff plate theory) was employed to perform the analytical calculation of the plate's critical buckling load. Additionally, since the plate is a layered structure, the necessary formulas were derived using the classical lamination theory. Parameters such as the plate's edge lengths, layer thickness, layer material, total number of layers, magnitude and ratio of the compressive loads in both directions were derived from a previously studied problem in the literature. Thus, the calculations were validated by comparing them with the results obtained in the literature.

Extensive studies on hybrid composites have demonstrated their superior design flexibility and mechanical properties compared to non-hybrid composites. In this purpose, a hybrid plate was created by employing carbon/epoxy and glass/epoxy materials. The positioning of plies with different material properties was carefully considered during the hybridization process and taking into account its impact on the plate's bending rigidity. Therefore, carbon/epoxy layers exhibiting higher bending rigidity were placed farther from the symmetry axis, whereas less rigid glass/epoxy layers were positioned closer to the symmetry axis. By employing this strategy, the elements of the bending rigidity matrix, which directly impact the critical buckling coefficient, were effectively maximized. The cost function was determined by utilizing previous works in the literature. Instead of using the actual material prices, the cost ratio of the two materials was calculated and incorporated into the equation.

Population optimization algorithms are powerful tools employed for solving complex problems. Different types of population optimization algorithms such as genetic algorithm, ant colony optimization (ACO) algorithm, differential evaluation (DE) algorithm. In this study, particle swarm optimization (PSO) was utilized. The primary motivation for selecting this algorithm arises from the demonstrated evidence from previous studies indicating its superior convergence speed and performance compared to other stochastic algorithms. The objective functions were defined as maximizing the buckling load, minimizing the cost function, and maximizing the difference between the first two natural frequency values. The weighted sum method and the ε constraint method were employed to solve the multi-objective optimization problem. Since the objective functions were conflicting, Pareto optimal solutions were obtained. The optimization was repeated with different load and aspect ratios to investigate the effects of these parameters on the results.

FİBER TAKVİYELİ KATMANLI HİBRİT KOMPOZİT PLAKALARIN PARÇACIK SÜRÜ ALGORİTMASI İLE ÇOK AMAÇLI OPTİMİZASYONU

ÖZET

Bu çalışmada, katmanlı hibrit kompozit yapıların eksenel basma yükleri altında parçacık sürü optimizasyonu yaklaşımı kullanılarak çok amaçlı optimizasyonu ele alınmıştır. Yapılan çalışmada, 64 katmandan oluşan basit mesnetli bir kompozit plaka, iki doğrultuda sabit eksenel basma yüklerine maruz bırakılmıştır.

Havacılıkta tasarım kısıtlarının başında ağırlık gelmektedir. Hafif yapılar sivil havacılıkta operasyonel maliyetlerin azaltılmasına, askeri havacılıkta uçağın görev mesafesinin artmasına olanak sağlamaktadır. Kompozitler gösterdikleri yüksek mukavemet/ağırlık oranıyla bir çok durumda metalik malzemelere üstünlük sağlamaktadırlar. Ağırlık kısıtı göz önüne alındığında havacılıkta sıklıkla ince cidarlı yapılar kullanılmaktadır. Yapılar inceldikçe hasar durumları yapının mukavemetinden daha çok stabilite kaynaklı olmaktadır. Bu stabilite hasar durumlarından en çok karşılaşılanı burkulma durumudur. Her yapı herhangi bir dış kuvvet etkisi altında kalmadan ağırlığı gereği titreşim yapma eğilimindedir. Yapı eğer kuvvetli rüzgar, aerodinamik etkiler gibi dinamik dış kuvvet frekanslarıyla çakışan bir doğal frekansa sahipse ve bu dış kuvvetler tarafından uyarılırsa rezonansa girebilir ve bu durum yapısal bütünlüğün bozulmasına sebep olabilir. Yapının rezonansa girmesini önlemek için yapının doğal frekans değerlerinin ölçülmesi gerekmektedir. Ayrıca yapısal sağlık izleme metodunda yapının ilk frekansıyla ilgilenilirken diğer modların ilk moda yakın olması ölçümü ve analizi zorlaştırmaktadır. Bahsedilen problemler göz önüne alındığında burkulma yükünün ve doğal frekans değerlerinin optimize edilebilmesi için öncelikle analitik olarak hesaplanabilmesi gerekmektedir.

Plakanın kritik burkulma yükünün analitik hesabının yapılabilmesi için klasik plaka teorisinden (Kirchoff plaka teorisi) yararlanılmıştır. Ayrıca plaka katmanlı bir yapıda olduğundan klasik laminasyon teorisi yardımıyla gerekli formüller türetilmiştir. Burada bahsedilen iki teoremdeki formüller birbirleri içinde kullanılarak dört tarafı basit mesnetli, katmanlı bir plaka için burkulma formülasyonu çıkarılmıştır. Plakanın ilk ve ikinci doğal frekansının elde edilmesi için plakanın serbest titreşim davranışını ifade eden formülden yararlanılmıştır. Bu formülasyon için plakanın yoğunluğu bilinmesi gerekmektedir ancak, hibrit plaka farklı malzemelerden oluştuğundan hibrit plaka için ayrı bir yoğunluk hesabı yapılmıştır. Plakanın kenar uzunlukları, katman kalınlığı, katman malzemesi, toplam katman sayısı, her iki yöndeki basma yüklerinin büyüklüğü ve birbirlerine oranı belirlenirken daha önce literatürde çalışılmış bir plakayla aynı özelliklere sahip olmasına dikkat edilmiştir. Böylece yapılan hesaplamalar literatürdeki çalışmalarla kıyaslanarak doğrulanabilmiştir.

Hibrit kompozitler üzerine yapılan çalışmalar, hibrit kompozitlerin hibrit olmayan kompozitlere göre daha esnek bir tasarıma ve daha iyi mekanik özelliklere sahip

olduğunu göstermiştir. Bu amaçla plaka karbon/epoksi ve cam/epoksi malzemelerinin hibritlenmesi ile oluşturulmuştur. Hibritleme işlemi yapılırken, farklı malzemeye sahip katmanların simetri eksenine mesafesinin plakanın eğilme rijitliğine doğrudan etkisi göz önüne alınmış ve bu sebeple eğilme rijitliği yüksek olan karbon/epoksi katmanlar simetri ekseninden uzağa yerleştirilmişlerdir. Görece daha az rijit olan cam/epoksi katmanlar ise simetri eksenine daha yakın konumlandırımışlardır. Böylece burkulma katsayısını doğrudan etkileyen eğilme rijitlik matrisinin elemanlarının oldukça yüksek bir değere sahip olması sağlanmıştır. Yapılan bazı çalışmalarda kullanılan malzeme sayısı arttırılarak farklı malzeme kombinasyonları elde edilmiştir ancak bu çalışmada havacılıkta en çok kullanılan katman malzemeleriyle çalışılması tercih edilmiştir. Hibritleme işleme katmanlı yapının yalnızca mekanik özelliklerini değil aynı zamanda maliyetini de doğrudan etkilemektedir. Maliyet fonksiyonu belirlenirken literatürde yapılmış olan çalışmalardan faydalanılmıştır. Malzemelerin gerçek fiyatlarını kullanmak yerine iki malzemenin maliyetleri oranlanarak bu oran hesaba dahil edilmiştir.

Popülasyon optimizasyon algoritmaları aday çözümlerden havuz oluşturarak tekrarlayıcı bir süreçle bu çözümlerin iyileştirilmesi prensibiyle çalışan, karmaşık problemlerin çözümünde kullanılan güçlü bir araçtır. Genetik algoritma, karınca koloni optimizasyonu algoritması, ayrık evrimsel algoritmalar gibi literatürde sıklıkla kullanılan farklı popülasyon optimizasyon algoritmaları mevcuttur. Bu çalışmada popülasyon optimizasyon algoritmalarından biri olan parçacık sürü optimizasyonu (PSO) kullanılmıştır. Bu algoritmanın seçilmesindeki temel motivasyon yapılan çalışmalarda algoritmanın benzerlerine kıyasla yakınsama hızı ve performans bakımından olumlu sonuçlar verdiğinin gösterilmiş olmasıdır. PSO algoritması çözüm uzayında rastgele bir sürü oluşturur ve bu sürüyü oluşturan her bir parçacığa bir konum ve hız bilgisi atanır. Bazı matematiksel ifadeler kullanılarak parçacığın konum bilgisi tekrarlamalı olarak güncellenir. Sürü içindeki kişisel en iyi ve küresel en iyi değerlerin belirlenmesi için her bir parçacığın uygunluk değeri hesaplanır. Çalışmanın içeriğinde algoritma detaylı bir şekilde anlatılmıştır. Algoritma MATLAB yazılım programında kodlanmıştır.

Amaç fonksiyonları burkulma yükünün maksimizasyonu, maliyet fonksiyonun minimizasyonu ve ilk iki doğal frekans değeri arasındaki farkın maksimizasyonu şeklinde belirlenmiştir. Çok amaçlı optimizasyon probleminin çözümünde ağırlıklı toplam (weighted sum) yöntemi ve ε kısıtlama yönteminden faydalanılmıştır. Ağırlıklı toplam yöntemi birbiriyle çelişen birden fazla amaç fonksiyonunu belirli katsayılarla çarpıp toplayarak tek bir uygunluk değeri bulunmasını sağlayan bir yöntemdir. Katsayılar değiştirilerek çözüm uzayında birçok nokta elde edilebilir. Katsayıalrın değişim miktarı azaltılarak alınan çözümün çözünürlüğü arttırılabilir. Diğer bir yöntem olan ε kısıtlama yönteminde ise amaç fonksiyonlarından biri optimize edilmek için seçilir ve geri kalan amaç fonksiyonları kısıt olarak hesaba dahil edilir. Bu çalışmada iki amaç fonksiyonun ele alındığı bir durumda bu iki metod ile Pareto optimal çözümler elde edilmiştir ve çözümler Pareto front eğrisi üzerinde gösterilmiştir. Her iki yöntemle benzer eğilimdeki sonuçların elde edilmesi sonuçların güvenilirliğini arttırmaktadır. Ardından üç amaç fonksiyonu ağırlıklı toplam yöntemiyle beraber incelenmiştir. İkiden fazla amaç fonksiyonunun olduğu problemlerde ε kısıtlama yönteminin efektif olmaması sebebiyle sadece ağırlıklı toplam yöntemi kullanılmıştır.

Üç amaç fonksiyonu artık çözüm eğrisi yerine bir çözüm yüzeyi (Pareto surface) elde edilmesini sağlar. Üç amaç fonksiyonlu Pareto optimal çözümlerde çeyrek küre yüzeyi elde edilmiştir. Bu yüzey üzerinden seçilecek herhangi bir nokta çözüm uzayında optimum sonucu vermektedir.

Son olarak farklı yük ve plaka açıklık oranlarıyla optimizasyon tekrarlanarak bu parametrelerin sonuçlar üzerindeki etkileri yorumlanmıştır. Bu amaçla yük oranını sabit tutarak üç adet ve açıklık oranını sabit tütarak üç adet durum oluşturulmuştur. Tüm bu durumların sonuçları tablolaştırılmış ve Pareto optimal çözümler figür halinde sunulmuştur. Açıklık oranı ve yük oranının dizilim ve kullanılan fiber malzemenin cinsi açısından öneme sahip olduğu gözlenmiştir. Pareto optimal çözümler sonrası benzer geometrik şekiller elde edilmiştir.

1. INTRODUCTION

In the aerospace industry, polymer matrix layered composites are widely preferred due to their high stiffness, durability, lightweight nature, superior corrosion and fatigue resistance, high impact strength, and their radar-absorbent properties, particularly in 5th generation fighter aircraft, when compared to traditional materials. The broadening scope of applications and growing importance of composite materials have led to increased research and the adoption of different composite materials in the industry. For instance, carbon/epoxy materials stand out due to their high strength and stiffness values, despite their high costs, while in applications where such high strength is not necessary, glass/epoxy is often preferred for its cost-effectiveness. At this point, the concept of producing hybrid composite materials by combining different fibers emerged. By employing hybridization techniques, the mechanical properties of composite materials can be enhanced, allowing for the design of structures with significantly increased strength relative to their weights. Furthermore, hybrid composites enable the production of the lowest cost composite that meets the requirements for stiffness and strength [1].

In the aerospace industry, thin-walled structures are frequently utilized, especially when weight constraints are considered. As structures become thinner, stability related failure criteria become more critical than strength related failure criteria. One of the most common stability related failure criteria is buckling. In orthotropic plates, one approach to enhancing buckling strength is to modify the stacking sequence instead of increasing thickness.

Another phenomenon that causes buckling is the excessive vibration of shell structures in resonance. Aircraft structures subjected to resonance exhibit unstable behavior and are susceptible to failure. In practice, to avoid these adverse conditions, the aim is to increase the value of the first natural frequency or to separate first two natural frequencies. A substantial gap between the first two natural frequencies effectively widens the operational range, mitigating the risk of resonance induced by external excitation [2]. In vibration health monitoring, the initial natural frequency signifies greater stiffness. However, overlapping natural frequencies can make it difficult to measure and analyze the correct resonance. For this reason, it is desirable to increase the gap between the first two natural frequencies [3].

1.1 Literature Review

Classical Lamination Theory (CLT) is the most widely adopted approach for designing structures with fibrous composite materials. Following the mid-20th century, numerous studies in the literature have been carried out about CLT. Through their work, Nettless [4], Berthelot [5], Ochsner [6] and Jones [7] successfully derived the equations for mechanical analysis of composite laminates. Jones additionally developed free vibration formulas for simply supported orthotropic plates. Leissa [8] presented buckling formulas for orthotropic plates subjected to diverse boundary conditions and loading case.

Hybrid composite research has began approximately 35 years ago. Duffy and Adali [9], pioneers in hybrid composite research, conducted a study in which they calculated the maximum buckling load for boron, kevlar, and glass fibers in both hybrid and non-hybrid configurations. The aim during the creation of hybrid composites was that the inner plies of hybrid composites comprised materials with low stiffness, while the outer plies consisted of high-stiffness composite materials. Thus, the objective was to produce cost-effective laminates. Variations in the maximum buckling load were observed by altering ply thicknesses to ensure laminates had equal mass.

Le Riche and Haftka [10] studied that the utilization of a genetic algorithm to optimize the stacking sequence of a composite laminate with the goal of maximizing buckling load. In the conducted study, a balanced four-ply laminate was aimed to achieve the maximum strain constraint under biaxial loading conditions while targeting the maximization of buckling load. The analytical formulation of the critical buckling load in terms of the flexural stiffness coefficients, was obtained from the relevant study. Also, the parameters of the genetic algorithm were modified to perform algorithm optimization. Haftka et al. [11] encoded each ply stacking sequence angle as a numerical value. Thus, the genetic algorithm was enabled to generate its population using this numerical sequence.

Eberhart and Kennedy [12] developed a new optimization algorithm which is called particle swarm optimization (PSO). This algorithm was developed inspired by the flocking behavior of herd animals. The application of the algorithm become widespread due to its reliance on fundamental mathematical operations and its computational efficiency in terms of memory consumption and execution speed. In their study Eberhart and Shi [13] identified parameter modifications that would facilitate the algorithm in achieving faster convergence.

Karakaya and Soykasap [1] indicate that how genetic algorithms (GA) and simulated annealing (SA) algorithms optimized results in increasing the values of natural frequency and buckling load of the laminate by altering the stacking sequence of hybrid composite plates. In this study, the effect of different aspect ratios and number of plies on hybrid and non-hybrid plates was examined. While solving a single-objective optimization problem, a pseudo objective function was defined, and in case of non-compliance with constraints, the penalty function method was applied.

Pal et al. [2] focused on optimizing the design of a laminated shell structure to maximize the difference between the first two consecutive frequencies by using genetic algorithm. Adali and Verijenko [14] investigated the free vibration analysis of a hybrid composite plate and the determination of its optimal stacking sequence in their study. Additionally, they derived an equation that allows for the determination of different mode shapes of a composite plate with simply supported boundary conditions. Li et al. [15] conducted a theoretical study on the free and forced vibration characteristics of carbon/glass hybrid composite laminated plates under various boundary conditions.

Spallino and Rizzo [16] defined a problem with multiple objective functions and applied it on a composite laminated structure. In their study, Suresh et al. [17] conducted multi-objective optimization of composite box beam structures, which are used in helicopter blades. Abachizadeh and Tahani [18] presented multi-objective optimization studies targeting the maximization of natural frequencies and minimization of costs on hybrid plates with varying aspect ratios and thickness values using the ACO algorithm. In order to calculate material costs, a dimensionless, relative cost function was defined. Cost ratio between carbon/epoxy and glass/epoxy materials specified as 8.

Yildiz and Lesieutre [19] obtained Pareto optimal results in their multi-objective optimization study using the PSO algorithm, employing both the weighted sum and ε constraint methods. In the weighted sum method, the importance of both objective functions is determined by coefficients w_1 and w_2 and by altering these coefficients, the problem is converted into a single-objective problem. Konak et al. [20] extended the weighted sum approach for more than two objective functions cases. In the ε constraint method, specific cost constraints are added to the analysis as limiting factors, thereby ensuring that the cost remains below the specified limit [19].

Serhat and Basdogan [21] utilized a multi-objective optimization approach with three distinct objective functions to achieve Pareto optimal outcomes for a laminated composite plate. These objectives aimed to maximize the torsional strength, first natural frequency, and stiffness of the plate. By graphically representing these functions, a Pareto surface was obtained.

1.2 The Scope of the Study

This study aims to perform a multi-objective optimization of the stacking sequence for a 64-ply hybrid composite plate, previously studied in the literature.

The objective functions can be listed as follows:

- Maximization of buckling load factor
- Maximization of the difference between the first and second natural frequencies
- Minimization of cost

This plate consisting of carbon/epoxy and glass/epoxy materials. Hybridization approach allows for the enhancement of buckling strength and stiffness of the plate by employing relatively costly carbon/epoxy layers, while the use of glass/epoxy helps balance composite cost.

The stacking sequence and ply angles of the laminate were considered as design variables, and plies with angles of 0°, ±45°, 90° degrees were used.

Particle swarm optimization algorithm was employed for the optimization process. Since simultaneously achieving multiple conflicting optimization functions is not feasible, the weighted sum and ε constraint methods were employed. When optimizing for two objective functions, the best design points can be represented by a line. Conversely, when optimizing for three objective functions, the best design points form a surface in the design space. Both of these scenarios were considered in this study. Finally, the study was extended to include plates with varying aspect ratios and loading ratios, and the influence of these parameters on the results was investigated.

In previous studies on hybrid composite plates in the literature, two different objective functions were examined, but Pareto optimal results were not obtained. In this study, in addition to previously investigated multi-objective optimization problems on hybrid composite plates, three different objective functions have been examined. The obtained Pareto optimal curves and Pareto optimal surfaces are presented graphically, and the results are also tabulated. Additionally, unlike previous studies, the effects of changes in the geometric properties of the plate and loading conditions on the results have been investigated.

2. MECHANICS OF COMPOSITE PLATES

The use of composite materials into civil aviation and military aviation has adhered to the standard procedure for implementing new technologies. The initial usage of composites was restricted to non-critical structural components, enabling the collection of valuable data from testing and operational experience to refine understanding of the material's behavior. This restrained application gradually expanded, initially focusing on smaller aircraft to leverage prior experience. In recent years, because of growing need for efficiency and cost reduction, composites have found broad application in larger aircraft [22].

The application of composites in the civil and military aviation industries over the years is shown in Figure 2.1 [22]. The percentage of structural weight attributed to composite materials has exhibited a similar increasing trend over the years in both civil and military aviation. Particularly in recent years, with the accumulation of experience in composites, the composite weight now exceeds half of the total structural weight.

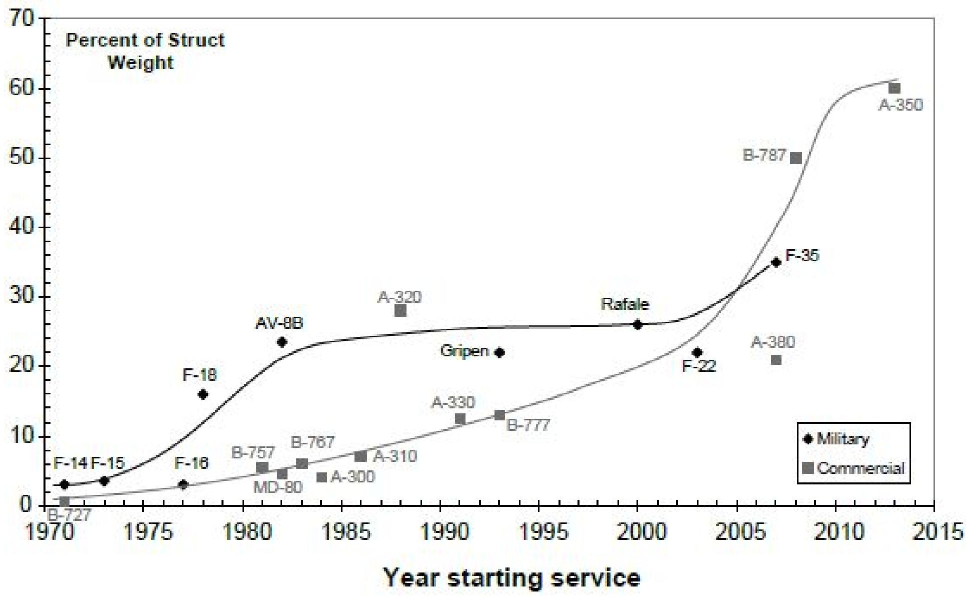

Figure 2.1 : The utilization of composites in the civil and military aviation industries [22].

2.1 Composite Materials

Composite materials consist of three primary constituents:

- The matrix component
- The reinforcement component
- Additive

The matrix constitutes a large portion of the volume of the composite. The matrix in a composite material acts like a glue, keeping the fibers together. It also helps distribute the loads between the fibers and protect them from the environmental damages. The reinforcement component also known as the fiber acts as the primary load-carrying element of the composite material. Fibers exhibit high strength particularly in the direction in which they are laid. Commonly used fiber materials can be listed as follows: carbon (graphite) fiber, glass fiber, aramid fiber, boron fiber, silicon carbid fiber, alumina fiber.

The arrangement of fibers, whether parallel or perpendicular to the principal axes of the material, significantly influences their strengths in those directions. Four types of fiber composites commonly used in aviation, unidirectional, bidirectional, discontinuous and woven, are shown in Figure 2.2 [23].

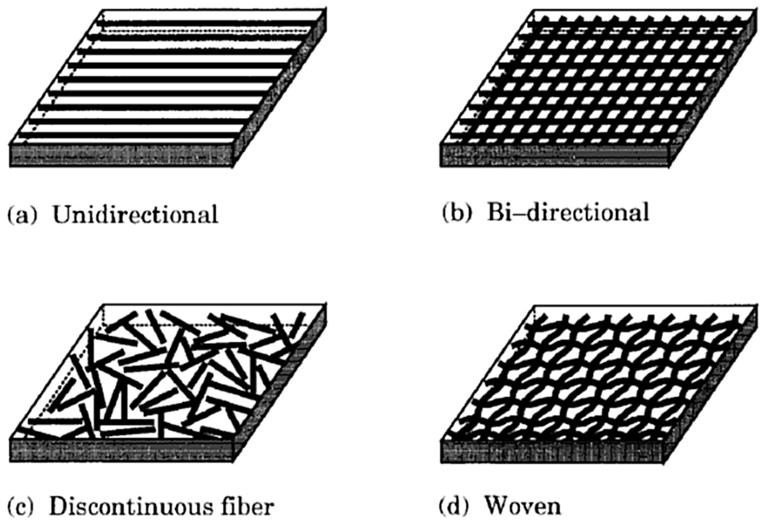

Figure 2.2 : Two types of lamina used in aviation [23].

The individual layers in the fiber composites were also named as laminas. A laminate is formed by stacking at least two laminas, with the same or varying fiber orientations. Figure 2.3 [24] illustrates a laminate structure composed of three layers. The orientation of each layer and the direction perpendicular to it by 90 degrees are denoted as the 1 and 2 directions, respectively. The stacking sequence of the laminate is defined by specifying the orientation of each lamina, starting from the bottom to the top of the laminate or vice versa. If the laminate is symmetric or has repetitive orientations, the stacking sequence can be simplified accordingly. Thus, multi-layer laminates can be easily expressed.

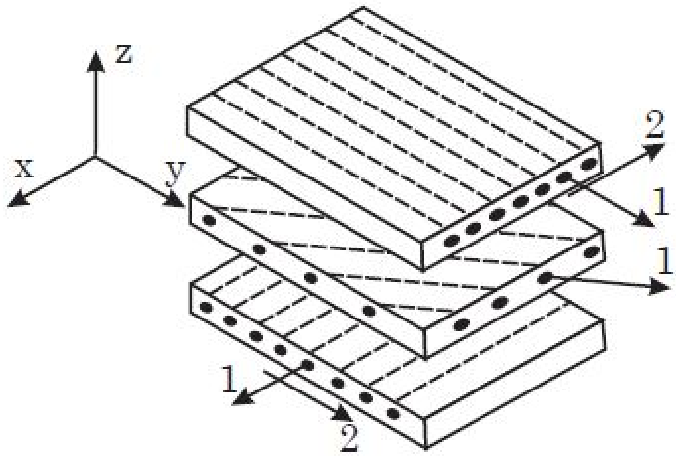

Figure 2.3 : The structure of the laminate [24].

In addition, all laminas constituting the laminate can have the same or different fiber materials. If all laminas have the same material, the structure can be referred to as a non-hybrid composite; otherwise, it can be named as a hybrid composite. In this study in order to achieve a balance between high mechanical performance and affordability, utilizes a hybridization method. This approach integrates carbon fibers for their high strength and stiffness with the glass fibers for their cost-efficiency.

2.2 Classical Lamination Theory (CLT)

The Classical Lamination Theory allows for the calculation of laminates based on the stress-strain behavior of the lamina, with the acceptance of certain assumptions. The formulas obtained in this section are based on the studies conducted by Nettless [4] and Jones [7].

The following assumptions should be made for CLT:

- The thickness of the laminate is significantly smaller than composite plate's edge dimensions.
- The layers of the laminate are supposed as completely bonded.
- During deformation, lines initially perpendicular to the laminate surface retain their straightness and perpendicularity relative to the deformed surface.
- Stress-strain and strain-displacement relations conforms to linear elastic behavior.
- There are insignificant transverse stresses and strains.

The stress-strain relationship derived from Generalized Hooke's Law can be applied to orthotropic plates as follows:

$$\begin{bmatrix} \sigma_1 \\ \sigma_2 \\ \tau_{12} \end{bmatrix} = \begin{bmatrix} Q_{11} & Q_{12} & 0 \\ Q_{12} & Q_{22} & 0 \\ 0 & 0 & Q_{66} \end{bmatrix} \begin{bmatrix} \varepsilon_1 \\ \varepsilon_2 \\ \gamma_{12} \end{bmatrix} \tag{2.1}$$

The matrix denoted by Q is defined as the reduced stiffness matrix, and its elements can be expressed as:

$$\begin{gathered} Q_{11} = \frac{E_1}{1-\nu_{12}\nu_{21}}, \quad Q_{22} = \frac{E_2}{1-\nu_{12}\nu_{21}}, \\ Q_{12} = \frac{\nu_{12}E_2}{1-\nu_{12}\nu_{21}} = \frac{\nu_{21}E_1}{1-\nu_{12}\nu_{21}}, \\ Q_{66} = G_{12} \end{gathered} \tag{2.2}$$

The force equilibrium of a lamina which is shown in Figure 2.4 subjected to loading at an angle other than the axial or perpendicular direction is obtained by using a free body diagram.

$$\begin{aligned} \sigma_1 &= \sigma_x \cos^2\theta + \sigma_y \sin^2\theta + 2\tau_{xy}\sin\theta\cos\theta \\ \sigma_2 &= \sigma_x \sin^2\theta + \sigma_y \cos^2\theta - 2\tau_{xy}\sin\theta\cos\theta \\ \tau_{12} &= -\sigma_x \sin\theta\cos\theta + \sigma_y \sin\theta\cos\theta + \tau_{xy}(\cos^2\theta - \sin^2\theta) \end{aligned} \tag{2.3}$$

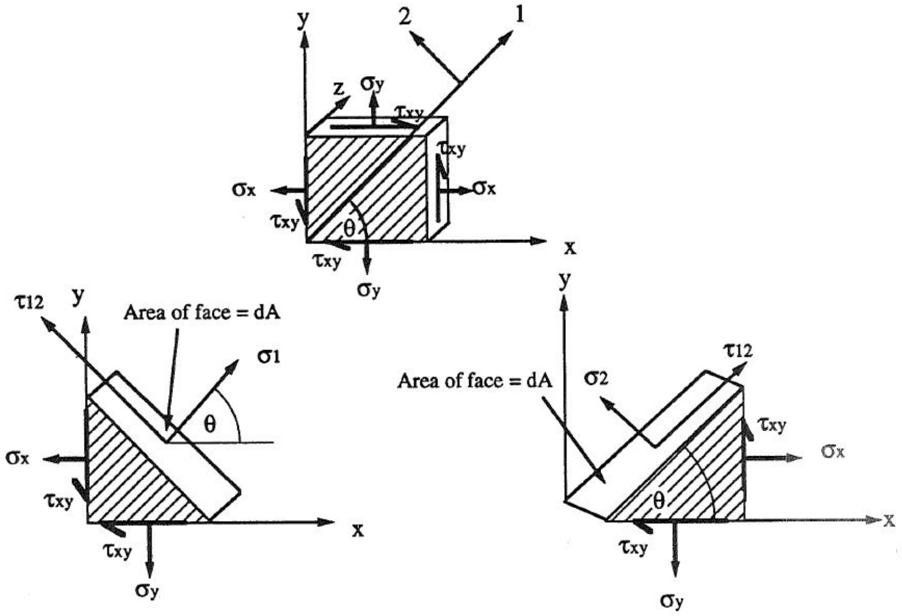

Figure 2.4 : Stress transformation in a body [4].

Equation 2.3 can be expressed in matrix form as below:

$$\begin{bmatrix}\sigma_1\\ \sigma_2\\ \tau_{12}\end{bmatrix} = \begin{bmatrix}\cos^2\theta & \sin^2\theta & 2\sin\theta\cos\theta\\ \sin^2\theta & \cos^2\theta & -2\sin\theta\cos\theta\\ -\sin\theta\cos\theta & \sin\theta\cos\theta & (\cos^2\theta-\sin^2\theta)\end{bmatrix}\begin{bmatrix}\sigma_x\\ \sigma_y\\ \tau_{xy}\end{bmatrix} \tag{2.4}$$

The 3x3 matrix derived in Equation 2.4 is referred to as the transformation matrix. This matrix allows the transformation between the 1-2 coordinate system and the x-y coordinate system. With Equation 2.1 and the transformation matrix, the following equality can be derived:

$$\begin{bmatrix}\sigma_x\\ \sigma_y\\ \tau_{xy}\end{bmatrix} = [T]^{-1}[Q]\begin{bmatrix}1&0&0\\0&1&0\\0&0&2\end{bmatrix}[T]\begin{bmatrix}1&0&0\\0&1&0\\0&0&1/2\end{bmatrix}\begin{bmatrix}\varepsilon_x\\ \varepsilon_y\\ \gamma_{xy}\end{bmatrix} \tag{2.5}$$

Consequently, a new matrix has been defined to characterize the stress-strain relationship. This matrix, which is reiterated in Equation 2.6, is referred to as the lamina stiffness matrix or Q-Bar matrix.

$$[\overline{Q}] = [T]^{-1}[Q]\begin{bmatrix}1&0&0\\0&1&0\\0&0&2\end{bmatrix}[T]\begin{bmatrix}1&0&0\\0&1&0\\0&0&1/2\end{bmatrix} \tag{2.6}$$

The elements of the Q-Bar matrix can be stated as follows:

$$\begin{aligned}
\overline{Q}_{11} &= Q_{11}c^4 + 2(Q_{12} + 2Q_{66})c^2s^2 + Q_{22}s^4 \\
\overline{Q}_{12} &= (Q_{11} + Q_{22} - 4Q_{66})c^2s^2 + Q_{12}(c^4 + s^4) \\
\overline{Q}_{22} &= Q_{11}s^4 + 2(Q_{12} + 2Q_{66})c^2s^2 + Q_{22}c^4 \\
\overline{Q}_{16} &= (Q_{11} - Q_{12} - 2Q_{66})c^3s + (Q_{12} - Q_{22} + 2Q_{66})cs^3 \\
\overline{Q}_{26} &= (Q_{11} - Q_{12} - 2Q_{66})s^3c + (Q_{12} - Q_{22} + 2Q_{66})sc^3 \\
\overline{Q}_{66} &= (Q_{11} + Q_{22} - 2Q_{12} - 2Q_{66})c^2s^2 + Q_{66}(c^4 + s^4)
\end{aligned} \tag{2.7}$$

where $c = \cos\theta$ and $s = \sin\theta$.

Therefore, the stress-strain relationship may be expressed as below:

$$\begin{bmatrix} \sigma_x \\ \sigma_y \\ \tau_{xy} \end{bmatrix} = \begin{bmatrix} \overline{Q}_{11} & \overline{Q}_{12} & \overline{Q}_{16} \\ \overline{Q}_{12} & \overline{Q}_{22} & \overline{Q}_{26} \\ \overline{Q}_{16} & \overline{Q}_{26} & \overline{Q}_{66} \end{bmatrix} \begin{bmatrix} \varepsilon_x \\ \varepsilon_y \\ \gamma_{xy} \end{bmatrix} \tag{2.8}$$

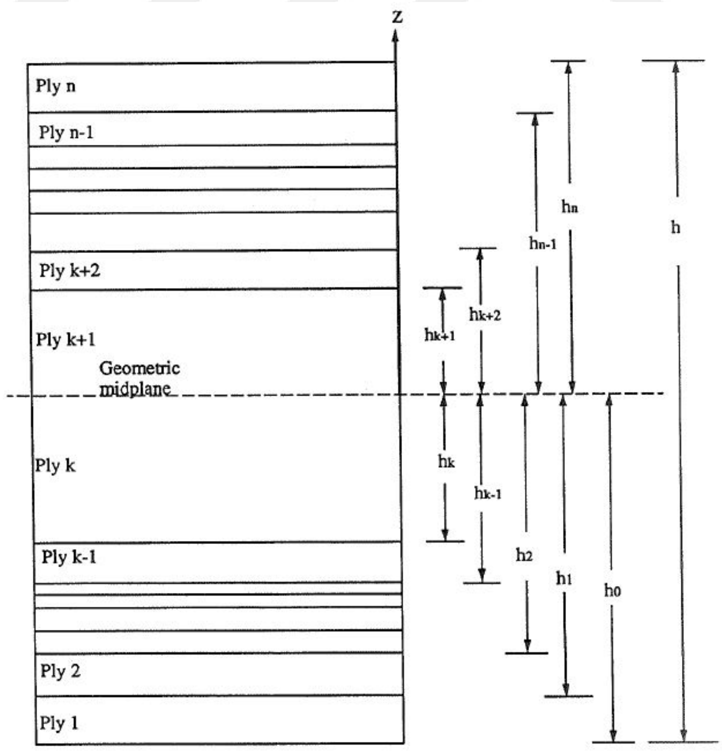

Figure 2.5 : Representation of N ply laminate [4].

Kirchhoff's theorem emphasizes that the strain varies linearly through the laminate thickness. Thus, the stress-strain relationship of the k-th layer of the n-th ply composite plate showed in Figure 2.5 can be formulated as follows:

$$\begin{bmatrix}\sigma_x\\ \sigma_y\\ \tau_{xy}\end{bmatrix} = \begin{bmatrix}\overline{Q}_{11} & \overline{Q}_{12} & \overline{Q}_{16}\\ \overline{Q}_{12} & \overline{Q}_{22} & \overline{Q}_{26}\\ \overline{Q}_{16} & \overline{Q}_{26} & \overline{Q}_{66}\end{bmatrix} \begin{bmatrix}\varepsilon_x^0\\ \varepsilon_y^0\\ \gamma_{xy}^0\end{bmatrix} + z \begin{bmatrix}\overline{Q}_{11} & \overline{Q}_{12} & \overline{Q}_{16}\\ \overline{Q}_{12} & \overline{Q}_{22} & \overline{Q}_{26}\\ \overline{Q}_{16} & \overline{Q}_{26} & \overline{Q}_{66}\end{bmatrix} \begin{bmatrix}\kappa_x\\ \kappa_y\\ \kappa_{xy}\end{bmatrix} \tag{2.9}$$

where $\left[\varepsilon^0\right]$ and $\left[\kappa\right]$ represents midplane strain and curvature of the plate respectively.

To determine the resultant force and moment acting on a laminate, the force and moment on each lamina must be integrated through the thickness. When the plate depicted in Figure 2.6 is considered, the resultant force and moment can be calculated as:

$$\begin{bmatrix}N_x\\ N_y\\ N_{xy}\end{bmatrix} = \int_{-h/2}^{h/2} \begin{bmatrix}\sigma_x\\ \sigma_y\\ \tau_{xy}\end{bmatrix} dz = \sum_{k=1}^{N} \int_{z_{k-1}}^{z_k} \begin{bmatrix}\sigma_x\\ \sigma_y\\ \tau_{xy}\end{bmatrix}_k dz \tag{2.10}$$

and

$$\begin{bmatrix}M_x\\ M_y\\ M_{xy}\end{bmatrix} = \int_{-h/2}^{h/2} \begin{bmatrix}\sigma_x\\ \sigma_y\\ \tau_{xy}\end{bmatrix} dz = \sum_{k=1}^{N} \int_{z_{k-1}}^{z_k} \begin{bmatrix}\sigma_x\\ \sigma_y\\ \tau_{xy}\end{bmatrix}_k z\,dz \tag{2.11}$$

Eq. 2.9 can be substituted in, Eq. 2.10, and Eq. 2.11. Then, due to $\left[\varepsilon^0\right]$ and $\left[\kappa\right]$ matrices are constant with respect to z (i.e., not functions of z), these matrices can be removed from the integrals. Thus the following equations has been derived:

$$\begin{aligned}\begin{bmatrix}N_x\\ N_y\\ N_{xy}\end{bmatrix} = \sum_{k=1}^{N} \begin{bmatrix}\overline{Q}_{11} & \overline{Q}_{12} & \overline{Q}_{16}\\ \overline{Q}_{12} & \overline{Q}_{22} & \overline{Q}_{26}\\ \overline{Q}_{16} & \overline{Q}_{26} & \overline{Q}_{66}\end{bmatrix}_k \begin{bmatrix}\varepsilon_x^0\\ \varepsilon_y^0\\ \gamma_{xy}^0\end{bmatrix} \int_{-h_{k-1}}^{h_k} dz \quad + \\ \begin{bmatrix}\overline{Q}_{11} & \overline{Q}_{12} & \overline{Q}_{16}\\ \overline{Q}_{12} & \overline{Q}_{22} & \overline{Q}_{26}\\ \overline{Q}_{16} & \overline{Q}_{26} & \overline{Q}_{66}\end{bmatrix}_k \begin{bmatrix}\kappa_x\\ \kappa_y\\ \kappa_{xy}\end{bmatrix} \int_{-h_{k-1}}^{h_k} z\,dz\end{aligned} \tag{2.12}$$

and

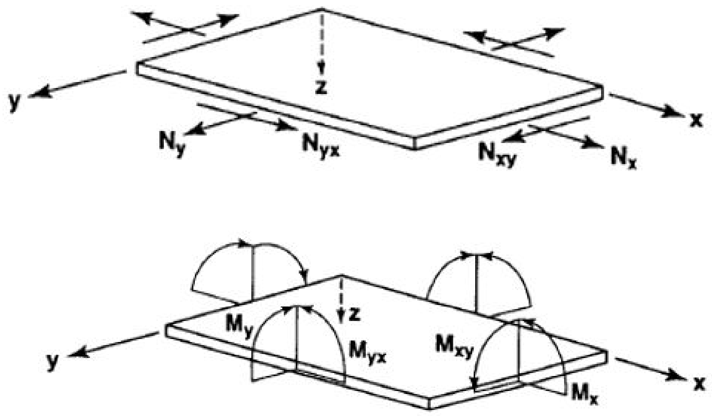

Figure 2.6 : Resultant force and moments on a flat laminate [7].

$$\begin{bmatrix} M_x \\ M_y \\ M_{xy} \end{bmatrix} = \sum_{k=1}^{N} \begin{bmatrix} \overline{Q}_{11} & \overline{Q}_{12} & \overline{Q}_{16} \\ \overline{Q}_{12} & \overline{Q}_{22} & \overline{Q}_{26} \\ \overline{Q}_{16} & \overline{Q}_{26} & \overline{Q}_{66} \end{bmatrix}_k \begin{bmatrix} \varepsilon_x^0 \\ \varepsilon_y^0 \\ \gamma_{xy}^0 \end{bmatrix} \int_{-h_{k-1}}^{h_k} z\,dz \quad + \\ \begin{bmatrix} \overline{Q}_{11} & \overline{Q}_{12} & \overline{Q}_{16} \\ \overline{Q}_{12} & \overline{Q}_{22} & \overline{Q}_{26} \\ \overline{Q}_{16} & \overline{Q}_{26} & \overline{Q}_{66} \end{bmatrix}_k \begin{bmatrix} \kappa_x \\ \kappa_y \\ \kappa_{xy} \end{bmatrix} \int_{-h_{k-1}}^{h_k} z^2\,dz \tag{2.13}$$

After integrating over the specified limits:

$$\begin{bmatrix} N_x \\ N_y \\ N_{xy} \end{bmatrix} = \sum_{k=1}^{N} \begin{bmatrix} \overline{Q}_{11} & \overline{Q}_{12} & \overline{Q}_{16} \\ \overline{Q}_{12} & \overline{Q}_{22} & \overline{Q}_{26} \\ \overline{Q}_{16} & \overline{Q}_{26} & \overline{Q}_{66} \end{bmatrix}_k \begin{bmatrix} \varepsilon_x^0 \\ \varepsilon_y^0 \\ \gamma_{xy}^0 \end{bmatrix} (h_k - h_{k-1}) \quad + \\ \begin{bmatrix} \overline{Q}_{11} & \overline{Q}_{12} & \overline{Q}_{16} \\ \overline{Q}_{12} & \overline{Q}_{22} & \overline{Q}_{26} \\ \overline{Q}_{16} & \overline{Q}_{26} & \overline{Q}_{66} \end{bmatrix}_k \begin{bmatrix} \kappa_x \\ \kappa_y \\ \kappa_{xy} \end{bmatrix} \frac{1}{2}(h_k^2 - h_{k-1}^2) \tag{2.14}$$

and

$$\begin{bmatrix} M_x \\ M_y \\ M_{xy} \end{bmatrix} = \sum_{k=1}^{N} \begin{bmatrix} \overline{Q}_{11} & \overline{Q}_{12} & \overline{Q}_{16} \\ \overline{Q}_{12} & \overline{Q}_{22} & \overline{Q}_{26} \\ \overline{Q}_{16} & \overline{Q}_{26} & \overline{Q}_{66} \end{bmatrix}_k \begin{bmatrix} \varepsilon_x^0 \\ \varepsilon_y^0 \\ \gamma_{xy}^0 \end{bmatrix} \frac{1}{2}(h_k^2 - h_{k-1}^2) \quad + \\ \begin{bmatrix} \overline{Q}_{11} & \overline{Q}_{12} & \overline{Q}_{16} \\ \overline{Q}_{12} & \overline{Q}_{22} & \overline{Q}_{26} \\ \overline{Q}_{16} & \overline{Q}_{26} & \overline{Q}_{66} \end{bmatrix}_k \begin{bmatrix} \kappa_x \\ \kappa_y \\ \kappa_{xy} \end{bmatrix} \frac{1}{3}(h_k^3 - h_{k-1}^3) \tag{2.15}$$

Finally, the following equations define the $[A],[B]$, and $[D]$ matrices:

$$[A]_{ij} = \sum_{k=1}^{N} [\overline{Q}_{ij}]_k (h_k - h_{k-1}) \tag{2.16}$$

$$[B]_{ij} = \frac{1}{2}\sum_{k=1}^{N} [\overline{Q}_{ij}]_k (h_k^2 - h_{k-1}^2) \tag{2.17}$$

$$[D]_{ij} = \frac{1}{3}\sum_{k=1}^{N} [\overline{Q}_{ij}]_k (h_k^3 - h_{k-1}^3) \tag{2.18}$$

$[A]$ is called the extensional matrix. The terms of the $[A]$ are related to normal stress and strains except A_{16}, A_{26} which are related to shear-extension coupling. $[B]$ is named as bending - extension coupling matrix. When the laminate exhibits a symmetrical stacking, all terms in the matrix equal to zero. Lastly, $[D]$ is called the bending stiffness matrix and $[D]$ establishes a direct relationship between the magnitude of plate curvatures and the corresponding bending moments.

The constitutive equation in a simple matrix form can be written as follows:

$$\begin{bmatrix} N \\ M \end{bmatrix} = \begin{bmatrix} A & B \\ B & D \end{bmatrix} \begin{bmatrix} \varepsilon^0 \\ \kappa \end{bmatrix} \tag{2.19}$$

2.3 Buckling of Simply Supported Laminated Plates

Classical Plate Theory derives analytical formulas by utilizing the Kirchoff assumptions for the plate (Figure 2.7 and Figure 2.8) under in-plane normal forces (N_x,N_y), in- plane shear (N_{xy}), shear forces (Q_x,Q_y), bending moments (M_x,M_y), and twisting moment (M_{xy}).

Taking into account the classical plate theory buckling equation for a homogeneous, orthotropic plate can be obtained as below [7]:

$$\begin{aligned} D_{11}\frac{d^4w}{dx^4} + D_{16}\frac{d^4w}{dx^3\,dy} + 2(D_{12}+2D_{66})\frac{d^4w}{dx^2\,dy^2} + 4D_{26}\frac{d^4w}{dx^2\,dy^2} \\ + D_{22}\frac{d^4w}{dy^4} = N_x\frac{d^2w}{dx^2} + 2N_{xy}\frac{d^2w}{dx\,dy} + N_y\frac{d^2w}{dy^2} \end{aligned} \tag{2.20}$$

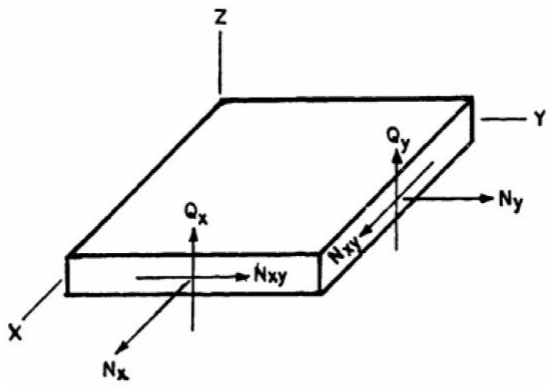

Figure 2.7 : Resultant stresses on a plate [8].

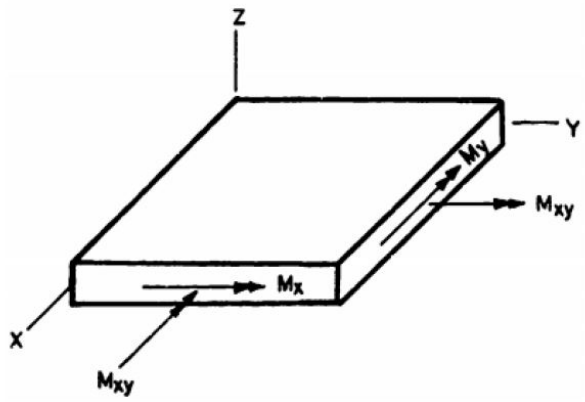

Figure 2.8 : Resultant moments on a plate [8].

Since Eq. 2.21 and Eq. 2.22 are satisfied the bending-twisting coupling terms, D_{16} and D_{26}, arising from off-axis layers have were neglected.

$$D_{16}(D_{11}^3 D_{22})^{-1/4} \leqslant 0.2 \tag{2.21}$$

$$D_{26}(D_{11} D_{22}^3)^{-1/4} \leqslant 0.2 \tag{2.22}$$

The following equation provides a description of vertical displacement w:

$$w(x,y) = \sum_m \sum_n A_{mn} \sin \frac{m\pi x}{a} \sin \frac{n\pi y}{b} \tag{2.23}$$

Boundary conditions for a plate (Figure 2.9) with all edges simply supported (SSSS) can be defined as follows:

$$
\begin{aligned}
x = 0; \quad & w(0,y) = 0; \quad M_x(0,y) = 0 \\
x = a; \quad & w(a,y) = 0; \quad M_x(a,y) = 0 \\
y = 0; \quad & w(x,0) = 0; \quad M_y(x,0) = 0 \\
y = b; \quad & w(x,b) = 0; \quad M_y(x,b) = 0
\end{aligned} \tag{2.24}
$$

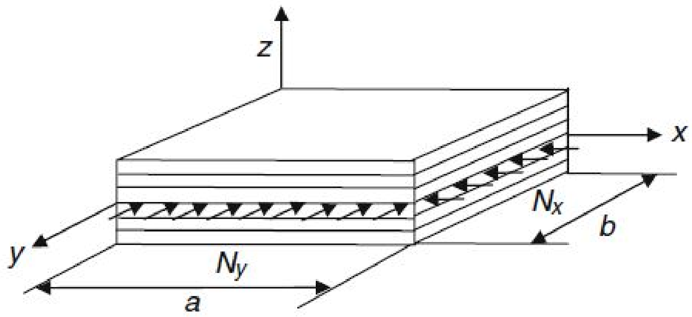

Figure 2.9 : Plate under biaxial loading.

Substituting Eq. 2.23 into Eq. 2.20 and solving the resulting differential equation with the boundary conditions specified in Eq. 2.24 yields the following generalized equation:

$$
N_x(\frac{m}{a})^2 + N_y(\frac{n}{b})^2 = -\pi^2 \left[D_{11}(\frac{m}{a})^4 + 2(D_{12} + 2D_{66})(\frac{m}{a})^2(\frac{n}{b})^2 + D_{22}(\frac{n}{b})^4 \right] \tag{2.25}
$$

With appropriate modifications, the equation becomes [7]:

$$
\lambda_b(m,n) = \pi^2 \frac{\left[m^4 D_{11} + 2(D_{12} + 2D_{66})(rmn)^2 + (rn)^4 D_{22}\right]}{(am)^2 N_x + (ran)^2 N_y} \tag{2.26}
$$

where λ_b represents the buckling coefficient, m and n represent the half-wave numbers in the x and y directions, respectively, D_{ij} denotes the elements of the plate's bending stiffness matrix, and r represents the plate's aspect ratio (a/b). To determine the critical buckling loads, the load factor presented here must be multiplied with the applied compressive loads. As one can see from Equation 2.26, the buckling coefficient varies depending on the values of m and n. Therefore, a new definition should be established, and the four cases where m and n take on the values 1 and 2 should be examined.

The smallest value among these critical buckling factors $\lambda_b(1,1)$, $\lambda_b(1,2)$, $\lambda_b(2,1)$, $\lambda_b(2,2)$ should be identified as the critical buckling factor ($\lambda_{c,b}$).

2.4 Vibration of Simply Supported Laminated Plates

In this section the free vibration analysis equations for a simply supported orthotropic plate were derived. To achieve this, the formulas obtained in the previous section were utilized.

The following equation describes the free vibration behavior of an orthotropic plate [7]:

$$\begin{gathered} D_{11}\frac{d^4w}{dx^4} + D_{16}\frac{d^4w}{dx^3\,dy} + 2(D_{12}+2D_{66})\frac{d^4w}{dx^2\,dy^2} + \\ 4D_{26}\frac{d^4w}{dx^2\,dy^2} + D_{22}\frac{d^4w}{dy^4} = \rho h \Omega^2 w \end{gathered} \tag{2.27}$$

In this equation, ρ, h, and Ω represent, the mass per unit area of the plate, the total thickness of the plate, and the vibration frequency respectively. The variable w, representing the displacement in the z-direction, was previously defined in Eq. 2.23. The bending-twisting coupling terms, D_{16} and D_{26}, arising from off-axis layers have were neglected.

Eq. 2.23 and Eq. 2.24 were integrated in Eq. 2.27, then the following eqution was found [7]:

$$\Omega^2(m,n) = (\pi^4/\rho)[D_{11}(\frac{m}{a})^4 + 2(D_{12}+2D_{66})(\frac{m}{a})^2(\frac{n}{b})^2 + D_{22}(\frac{n}{b})^4] \tag{2.28}$$

Similar to a buckling formula, Eq. 2.28 produces different results based on the values chosen for m and n. The minimum value was obtained when m and n are both equal to one, which corresponds to the first natural frequency or fundamental frequency. The computation of natural frequencies was repeated for different m and n values to determine the frequency separation.

Since hybrid laminates are composed of multiple ply material, the density calculation was performed based on Eq. 2.29.

$$\rho = \frac{K_c\rho_c + K_g\rho_g}{K_c + K_g} \tag{2.29}$$

where;

K_c and K_g stand for number of carbon and glass fiber in the laminate and ρ_c and ρ_g represent density of the carbon and glass fiber respectively.

3. OPTIMIZATION TECHNIQUES

3.1 Introduction

Structural engineers prioritize achieving peak efficiency in their designs for various structures, ranging from civil infrastructure to spacecraft. The success of a design is evaluated based on its suitability for the intended purpose, often centered on strength or stiffness. To ensure the efficiency, resource consumption must also be carefully considered. Weight and cost typically serve as the primary metrics for resource consumption [25].

In recent decades, structural design has witnessed the rise of mathematical optimization as a powerful problem solving approach. This powerful methodology enables the optimization of designs by determining solutions that achieve the best possible outcome, considering specific design goals and limitations.

The first form of optimization involves minimizing or maximizing a single-objective function. Due to the reasons mentioned above, the most of the realistic engineering applications deal with the optimization of multiple design objectives. Since achieving an absolute optimal solution for each objective simultaneously is often impractical, multi-objective optimization strategies employ Pareto optimal solutions as a pragmatic approach.

Stochastic optimization techniques, such as differential evolution, genetic algorithms, and simulated annealing, are frequently utilized for the optimization of laminated composite plates. In this study, the particle swarm optimization algorithm, coded in MATLAB software, was used.

3.2 Single-Objective Optimization

The general formulation of a single-objective optimization problem can be expressed as follows:

$$
\begin{aligned}
&\text{Minimize} \quad F(X) \\
&\text{Subject to} \quad g_j(X) \leq 0 \quad \text{for} \quad j = 1, n_c \\
&X_i^l \leq X \leq X_i^u
\end{aligned}
\tag{3.1}
$$

where $F(X)$ is the objective function, $g_j(X)$ is the constraint, n_c is the number of constraint, X is the design variable and $X_i^l \leq X \leq X_i^u$ represent the upper and lower bound of the design variable.

In this study, a penalty approach [26] based on the principle of adding a large number relative to the fitness value if any of the constraints defined at the beginning of the optimization process are violated, was implemented. As defined in Eq.3.2, $F(X)$ represents the original objective function, r_p is the coefficient that increases the value of the penalty function, and $P(X)$ represents the penalty function.

$$
\Phi(X, r_p) = F(X) + r_p P(X) \tag{3.2}
$$

where

$$
P(X) = \sum_{j=1}^{n_c} max(0, g_j(X)) \tag{3.3}
$$

Increasing the value of r_p causes the probability of satisfying the constraints; however, this may lead to an inability to converge to the objective function.

3.3 Multi-Objective Optimization

Multi-objective optimization problems involve simultaneously optimizing multiple objectives, often with conflicting goals. To achieve optimal design for composite laminated plates, efficient methods for multi-objective optimization are necessary. These methodologies enable the identification of optimal design parameters within the specified design space. In this study, the weighted sum and ε constraint methods were employed.

Similar to single-objective optimization the general formulation of a multi-objective optimization problem can be expressed as follows:

$$\begin{aligned} &\text{Minimize} \quad F_1(X), F_2(X), \ldots, F_n(X) \\ &\text{Subject to} \quad g_j(X) \leq 0 \quad \text{for} \quad j = 1, n_c \\ &X_i^l \leq X \leq X_i^u \end{aligned} \tag{3.4}$$

As one can see, in Eq. 3.4 n number objective functions were minimized simultaneously.

3.3.1 Weighted sum method

All considered objective functions can be combined into a single-objective problem by multiplying them by specific coefficients and summing them up. This method can be represented as follows:

$$\begin{aligned} F(X) &= w_1 F_1(X) + w_2 F_2(X) + \ldots + w_n F_n(X) \\ \sum(w_1 &+ w_2 + \ldots + w_n) = 1 \end{aligned} \tag{3.5}$$

By modifying the coefficients, the impact of each objective function on the solution can be seen. The number of points within the solution space can be controlled by varying the degree of change applied to the coefficients.

3.3.2 ε constraint method

The ε constraint method tackles multi-objective optimization problems by prioritizing one objective function for optimization. The remaining objectives are then converted into constraints. This method can be written as below:

$$\begin{aligned} \text{Minimize} \quad & F_1(X) \\ \text{Subject to} \quad & F_2(X) \leq \varepsilon_2 \\ & F_3(X) \leq \varepsilon_3 \\ & \vdots \\ & F_n(X) \leq \varepsilon_n \end{aligned} \tag{3.6}$$

3.4 Particle Swarm Optimization

In this study, the Particle Swarm Optimization (PSO), one of the a heuristic optimization technique, was employed. The algorithm was developed in 1995 by

Eberhart and Kennedy, drawing inspiration from the collective behavior of flocking animals. Similar to genetic algorithms, the optimization process begins with a population (swarm) of randomly generated solutions. Each individual (particle) in the swarm iteratively attempts to converge to a predetermined fitness value (objective function). Potential solutions are updated based on the current best solutions within the swarm [12].

The PSO algorithm initializes a random swarm in the solution space, assigning each particle within this swarm with position and velocity value. The particle's position information is iteratively updated using specific mathematical expressions. The fitness value of each particle is calculated to determine the personal best and global best values within the swarm. The velocity and position information of the particles are updated according to the following mathematical expressions:

$$v_{ij}^{k+1} = w \times v_{ij}^{k} + c_1 \times r_1 \times (p_{ij}^{k} - x_{ij}^{k}) + c_2 \times r_2 \times (g_j^{k} - x_{ij}^{k}) \tag{3.7}$$

$$x_{ij}^{k+1} = x_{ij}^{k} + v_{ij}^{k+1} \tag{3.8}$$

In the equations, x_{ij}^k and v_{ij}^k stand for the position and velocity information of particle i^{th} in the j^{th} direction, respectively. The superscript k denotes the iteration number, while r_1 and r_2 represent randomly generated numbers between 0 and 1. p_{ij} represents the j^{th} component of particle i^{th}'s best position, while g_j denotes the j^{th}component of the best position obtained for the entire swarm up to the k^{th} iteration. The operation of the algorithm based on the movement of a particle is illustrated in Figure 3.1.

In Equation 3.7, w referred to as the inertia weight, is used to adjust the influence of the particle's previous-step velocity vector on its next-step velocity vector. In the study conducted by Eberhart and Shi [13], it was noted that a linear decrease in the inertia weight, ranging from 0.9 to 0.4 in each iteration, positively affected the convergence speed of the algorithm.

The coefficients c_1 and c_2 respectively denote the personal learning coefficient (personal acceleration factor) and global learning coefficient (global acceleration

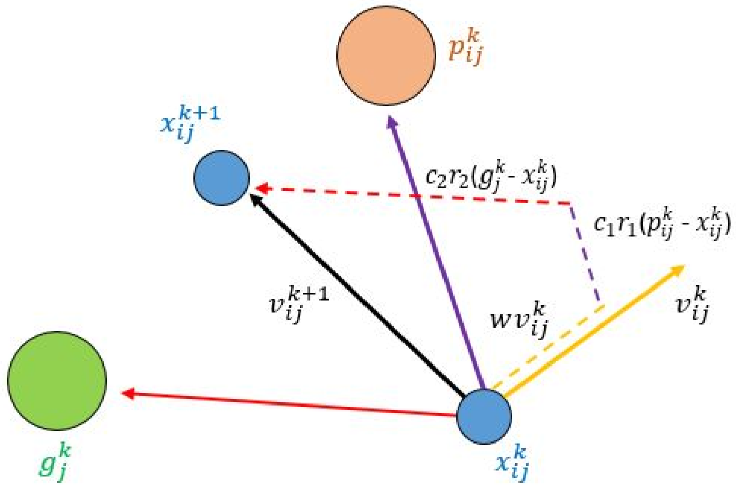

Figure 3.1 : PSO algorithm particle movement.

factor), both set to a value of 2. Increasing these values allows the particles to converge more rapidly to their personal best and global best positions [12].

The values of the parameters employed in the algorithm can be obtained from Table 3.1.

Table 3.1 : PSO parameters.

Parameter Name	Parameter Value
Inertia Weight Max.	0.9
Inertia Weight Min.	0.4
Personal Learning Coefficient	2
Global Learning Coefficient	2
Maximum Number of Run	10
Maximum Number of Iteration	100
Population Size	200

A comprehensive overview of the PSO algorithm is presented in the form of a flowchart in Figure 3.2.

3.4.1 Generating design variable

Firstly, the number of variables required to define the layer arrangement should be determined, in order to identify the boundary values for the particles. While, N total number of layers, θ layer orientation angle, it was decided to use $\pm\theta$ layers together. Also symmetric laminates were preferred. Thus, the total design variables decreased from N to $N/4$. Only $0^\circ_2, \pm45^\circ_2, 90^\circ_2$ layer angles were used in the design, and

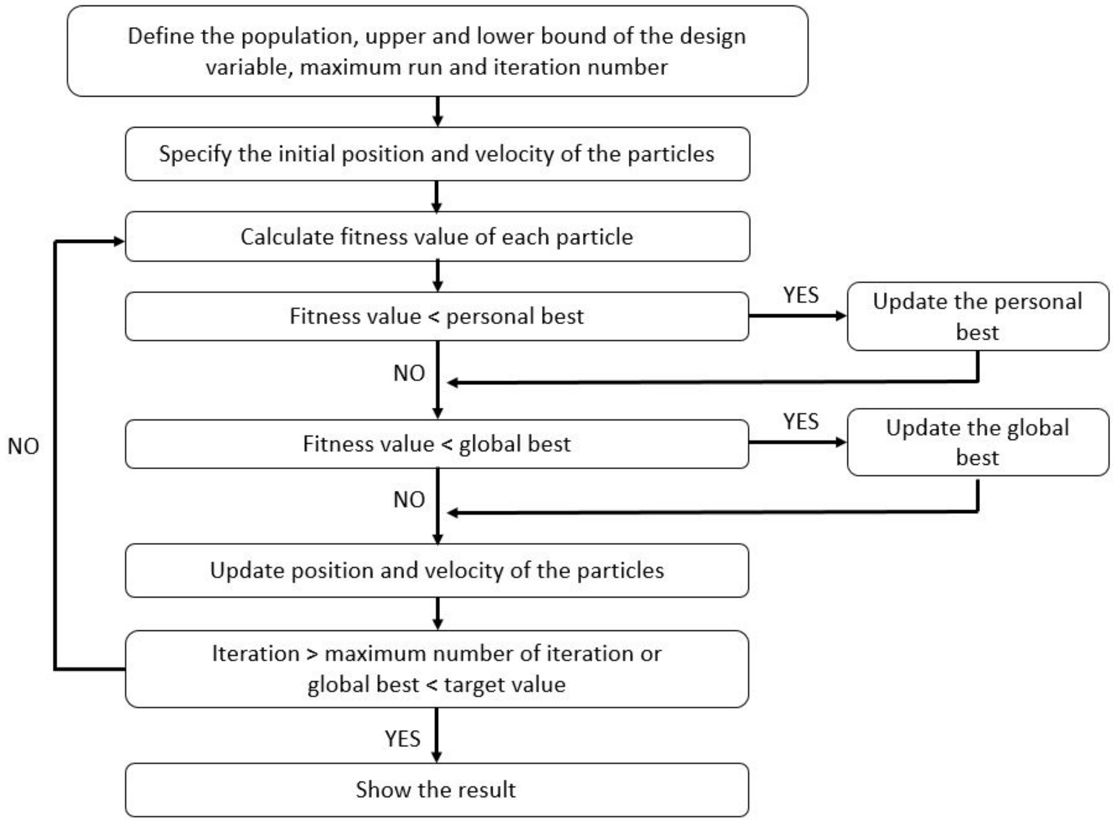

Figure 3.2 : PSO algorithm flowchart.

these angles were represented by 1, 2, and 3, respectively. For instance, the stacking sequence $[0^\circ_2/\pm45^\circ_2/90^\circ_2/\pm45^\circ_2/\pm45^\circ_2/90^\circ_2]_s$ was coded as $[1232_23]_s$.

3.5 Formation of Hybrid Plates

Figure 3.3 illustrates the hybridization approach utilized in this study. In this approach, carbon/epoxy layers with high flexural rigidity were always positioned in the outermost layers. This aims to maximize the flexural rigidity matrix. K_c and K_g represent the number of layers in which carbon/epoxy and glass/epoxy materials were used, respectively.

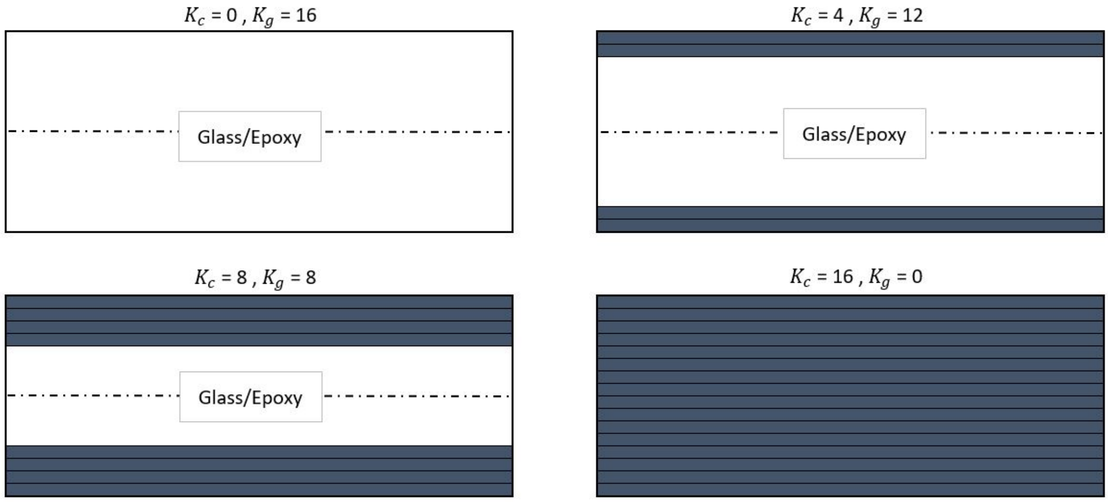

Figure 3.3 : Hybridization of composite plate.

3.6 Formation of Cost Function

The dimensionless relative cost function can be represented as follows [18]:

$$C = (1000)ab\frac{h}{N}g(\rho_g K_g + \alpha_0 \rho_c K_c) \tag{3.9}$$

Equation 3.9 presents the dimensionless relative cost function C of the hybrid plate, where a and b represent the plate's length and width, respectively; h represents the total thickness; N represents the total number of layers; g represents the gravitational acceleration (9.81 m/s^2); ρ_g and ρ_c denote the densities of the glass and carbon layers, respectively; K_g represents the number of glass layers; K_c represents the number of carbon layers; and α_0 represents the cost ratio of the two materials per unit weight. In this study, instead of using actual material prices, a cost ratio calculation was performed, and this ratio was assumed to be 8 since carbon/epoxy is approximately 8 times more expensive than glass/epoxy [18].

4. RESULTS AND DISCUSSION

4.1 Problem Statement

This section presents multi-objective optimization problems for laminated composite plates that have been previously studied in the literature in order to verify the PSO algorithm. The dimensions of the selected plate are $a = 0.508$ m, $b = 0.254$ m, layer thickness $t = 0.127$ mm, total number of layers $N = 64$, and applied compressive loads $N_x = N_y = 1$ N/m. Carbon/epoxy and glass/epoxy materials, whose mechanical properties can be found in Table 4.1, were used for the hybridization approach.

Table 4.1 : Material properties [1].

Property	Glass/epoxy	Carbon/epoxy
Elasticity modulus, E_1 (GPa)	38.6	181
Elasticity modulus, E_2 (GPa)	8.27	10.3
Shear modulus, G_{12} (GPa)	4.14	7.17
Poisson ratio, ν_{12}	0.26	0.28
Density, ρ (kg/m^3)	1800	1600

Initially, two objective functions were considered: buckling load maximization and cost minimization. Pareto optimal solutions were obtained using the weighted sum and ε constraint methods, as discussed in Section 3.3. The results were visualized on the Pareto front curve, and their consistency was evaluated. Subsequently, the third objective function, frequency separation maximization, was incorporated into the analysis. Due to the increased complexity of the ε constraint method with three objective functions, the weighted sum method was retained. Finally, the study was extended to plates with different aspect ratios $a/b = 1$, $a/b = 2$, $a/b = 1/2$ and different loading ratios, $N_x/N_y = 1$, $N_x/N_y = 2$, $N_x/N_y = 1/2$. Impact of these parameters on the results was discussed.

4.2 Results

4.2.1 Two objective function

Tables 4.2 and 4.3 summarize the results obtained using the weighted sum method and the ε constraint method, respectively. In the weighted sum method, the relative importance of each objective function was determined by the weights w_1 and w_2. The laminate stacking sequence and the total number of carbon/epoxy layers were tabulated by varying these weights. It was observed that as the importance of the cost function decreased, the utilization of carbon/epoxy, which has a higher cost ratio, increased. When the laminate stacking sequence was examined it can be seen that the algorithm favored layers with orientations of $\pm 45^\circ_2$ and 90°_2 over 0°_2 layers.

In the ε constraint method, specific cost constraints were added as limitations to the analysis to ensure that the cost remained below a predetermined limit. The laminate stacking sequence and the number of carbon/epoxy layers were obtained by incrementally increasing the cost limit in each step. As the limit increased, more carbon/epoxy was used in the optimal solution.

Table 4.2 : Buckling load factor and the cost, weighted sum method.

Buckling load factor weight (w_1)	Cost weight (w_2)	Buckling load factor	Cost	Stacking Sequence	K_c
0	1	194428.65	18519.22	$[2_2 3213_2 232321212]_s$	0
0.1	0.9	713223.05	53885.78	$[3_3 2_2 3_{11}]_s$	20
0.2	0.8	868530.02	78642.37	$[3_2 2_2 3_4 23_3 2_2 3_2]_s$	34
0.3	0.7	912187.24	92789.00	$[3_2 2_2 3_4 23_2 2_2 323]_s$	42
0.4	0.6	925017.83	99862.31	$[3_2 2_2 3_4 23_2 23_2 23]_s$	46
0.5	0.5	933336.31	106935.62	$[3_3 23_2 2_2 32_3 3232]_s$	50
0.6	0.4	936089.51	110472.28	$[3_4 232_3 32_3 32_2]_s$	52
0.7	0.3	937997.22	114008.93	$[3_3 2_2 3_3 23_2 2_2 3231]_s$	54
0.8	0.2	940091.14	121082.25	$[23_2 23_8 2_3 1]_s$	58
0.9	0.1	940091.14	121082.25	$[23_2 23_8 2_3 1]_s$	58
1	0	940665.47	131692.21	$[3_2 2_2 3_3 23_5 23_2]_s$	64

Figure 4.1 displays the Pareto front curve and the Pareto optimal results obtained using these two methods. When the buckling load factor is maximized, the cost

Table 4.3 : Buckling load factor and the cost, ε constraint method.

Cost constraint (ε)	Cost	Buckling load factor	Stacking Sequence	K_c
≤ 50000	46812.47	645609.46	$[23_9 232_2 3_2]_s$	16
≤ 62000	60959.09	769800.44	$[323_3 23_{10}]_s$	24
≤ 74000	71569.06	835835.52	$[3_3 232_2 3_7 2_2]_s$	30
≤ 86000	85715.68	893739.99	$[23_5 2323_2 23_3 1]_s$	38
≤ 98000	96325.65	919318.21	$[3_4 2_2 32_2 32_2 3_3 2]_s$	44
≤ 110000	106935.62	933366.36	$[3_2 23_2 2_2 3_3 23_5]_s$	50
≤ 122000	121082.25	940113.39	$[323_2 23_4 2_2 3_3 2_2]_s$	58
≤ 136000	131692.21	940665.47	$[3_2 2_2 3_3 23_5 23_2]_s$	64

correspondingly increases along the Pareto front curve. The similar trends observed with both methods enhance the reliability of the results.

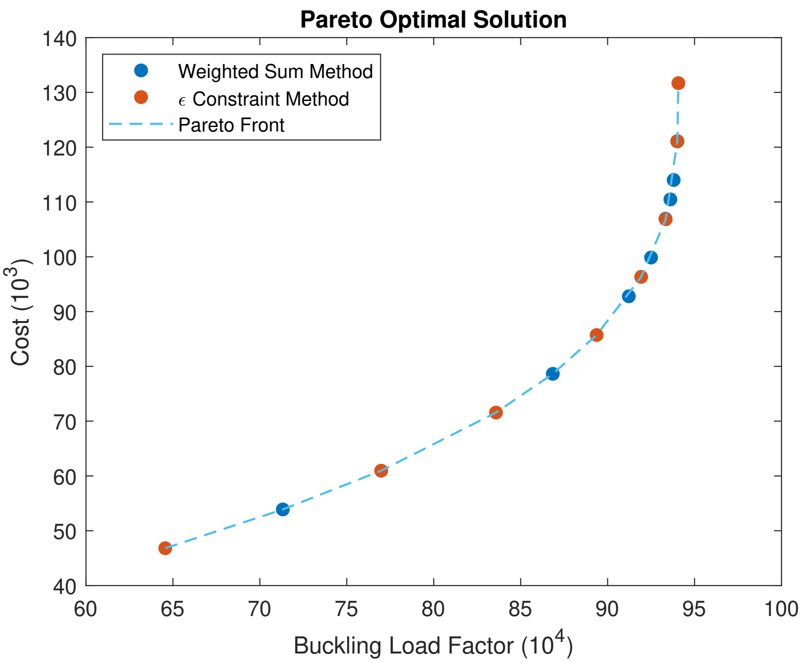

Figure 4.1 : Pareto optimal results for two objective function.

4.2.2 Three objective function

At this stage, the third objective function, which involves maximizing the difference between the first two natural frequencies, in other words, frequency separation maximization, has been included in the calculation. For each of the three functions, three weight factors were defined at every step. In order to increase the resolution of the solution more results was obtained. To achieve this, the optimization code was modified so that the weight factor changed by 0.025 at each step. Consequently, 856 different scenarios were examined in the solution space. Only specific coefficients were selected and tabulated in Table 4.4. All obtained results are provided in Appendix A.

In the initial studies, it was observed that the difference between the first two natural frequencies was an order of magnitude lower than the values of the buckling load factor and cost. To observe the effect of this function in the weighted sum method, the relevant function was multiplied by 100 and this value was presented in the Table 4.4.

Table 4.4 : Three objective function, weighted sum method.

Buckling load factor weight (w_1)	Cost weight (w_2)	Frequency sep. weight (w_3)	Buckling load factor	Cost	Frequency separation	Stacking Sequence	K_c
0	0	1	176527.64	131692.21	268975.70	$[1_{11}2121_2]_s$	64
0	0.2	0.8	174428.31	110472.28	265225.35	$[1_{11}21321]_s$	52
0	0.4	0.6	163712.87	82179.03	253650.52	$[1_{10}2_212_23]_s$	36
0	0.6	0.4	144019.21	57422.44	228064.78	$[1_{16}]_s$	22
0	0.8	0.2	101751.13	25592.53	147764.01	$[1_{16}]_s$	4
0	1	0	139146.97	18519.22	104278.74	$[1_22_3131_22_61]_s$	0
0.2	0	0.8	700693.13	131692.21	235315.81	$[2_{16}]_s$	64
0.2	0.2	0.6	697280.36	110472.28	232013.85	$[2_{16}]_s$	52
0.2	0.4	0.4	684893.28	96325.65	228117.93	$[2_{16}]_s$	44
0.2	0.6	0.2	903766.65	89252.34	94373.20	$[3_4232_43_2232_2]_s$	40
0.2	0.8	0	868528.11	78642.37	92027.79	$[3_223_22323_22_3323]_s$	34
0.4	0	0.6	940647.25	131692.21	98559.41	$[23_62_33_323_2]_s$	64
0.4	0.2	0.4	938029.11	114008.93	97436.45	$[3_32_23_223_22_2323_2]_s$	54
0.4	0.4	0.2	933366.36	106935.62	96837.87	$[23_423_32323_4]_s$	50
0.4	0.6	0	925092.95	99862.31	96016.43	$[3_223_2232323_323_2]_s$	46
0.6	0	0.4	940647.25	131692.21	98559.41	$[3_223_32_232_23_5]_s$	64
0.6	0.2	0.2	939083.98	117545.59	97842.72	$[3_22_23_52_23_223_2]_s$	56
0.6	0.4	0	936046.45	110472.28	97180.65	$[323_223_223_8]_s$	52
0.8	0	0.2	940665.47	131692.21	98509.78	$[3_2232323_523_3]_s$	64
0.8	0.2	0	940091.14	121082.25	97908.80	$[23_432_23_42323]_s$	58
1	0	0	940647.25	131692.21	98559.41	$[323_223_323_32_23_2]_s$	64

According to Table 4.4, as the weight factor of the buckling load factor increases, 90°_2 plies are preferred over 0°_2 plies. Conversely, for maximum frequency separation, the opposite trend was observed. Additionally, an increasing weight factor for the cost function resulted in a higher usage of glass fibers.

In Figure 4.2, it is observed that the Pareto optimal results correspond to the surface of a quarter-sphere in the solution space. Any point chosen on this surface represents an optimal solution for the problem. The reason for observing less than 856 points in the figure is due to overlapping results.

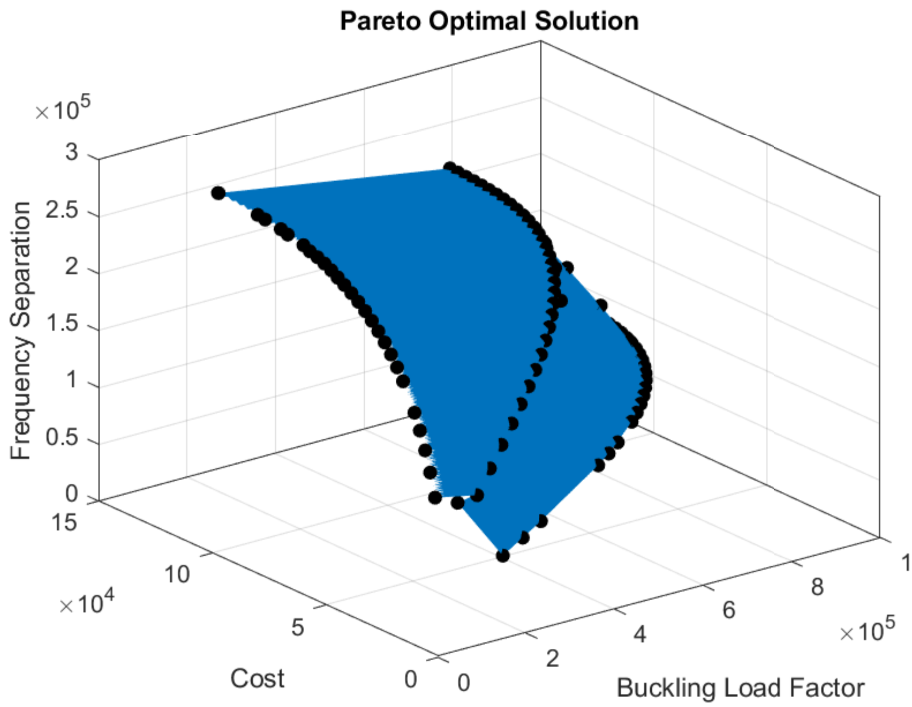

Figure 4.2 : Pareto optimal results for three objective function.

4.2.3 Effect of aspect ratio

In order to observe the effect of the panel's aspect ratio on the results, the design cases shown in Table 4.5 were examined. When determining the edge lengths of the panel, the goal was to keep the product of a and b, which represents the area of the plate, constant. Since the cost function is directly dependent on the area of the plate, ensuring a similar impact of the cost function on the outcome was targeted during comparisons. The load case ratio was kept constant.

Table 4.5 : Design cases DC1.

Design Case	Load Ratio	a [m]	b [m]	Aspect Ratio
DC1a	1	0.254	0.508	0.5
DC1b	1	0.359	0.359	1
DC1c	1	0.508	0.254	2

Table 4.6 and Figure 4.3 present the results for DC1a, while Table 4.7 and Figure 4.4 show the results for DC1b. The results for DC1c were previously shown in Table 4.4 and Figure 4.2.

Table 4.6 : DC1a, weighted sum method.

Buckling load factor weight (w_1)	Cost weight (w_2)	Frequency sep. weight (w_3)	Buckling load factor	Cost	Frequency separation	Stacking Sequence	K_c
0	0	1	176527.64	131692.21	268975.70	$[3_{11}23232_2]_s$	64
0	0.2	0.8	174428.31	110472.28	265225.35	$[3_{11}23123]_s$	52
0	0.4	0.6	163674.29	82179.03	253668.32	$[3_{10}2_232_23]_s$	36
0	0.6	0.4	144019.21	57422.44	228064.78	$[3_{16}]_s$	22
0	0.8	0.2	101751.13	25592.53	147764.01	$[3_{16}]_s$	4
0	1	0	208544.34	18519.22	74039.57	$[1_22_3131_22_61]_s$	0
0.2	0	0.8	700693.13	131692.21	235315.81	$[2_{16}]_s$	64
0.2	0.2	0.6	697280.36	110472.28	232013.85	$[2_{16}]_s$	52
0.2	0.4	0.4	684893.28	96325.65	228117.93	$[2_{16}]_s$	44
0.2	0.6	0.2	903778.29	89252.34	94408.07	$[1_22_21_421_42_21]_s$	40
0.2	0.8	0	868618.88	78642.37	92021.36	$[121_42_21_42_213]_s$	34
0.4	0	0.6	940647.25	131692.21	98559.41	$[1_221_32_212_21_5]_s$	64
0.4	0.2	0.4	938029.11	114008.93	97436.45	$[121_52_41_221_2]_s$	54
0.4	0.4	0.2	933364.66	106935.62	96831.89	$[1_42_41_421_3]_s$	50
0.4	0.6	0	925071.47	99862.31	96050.94	$[1_4212_412_21_3]_s$	46
0.6	0	0.4	940647.25	131692.21	98559.41	$[1_32_31_62_21_2]_s$	64
0.6	0.2	0.2	939083.98	117545.59	97842.72	$[21_62_31_321_2]_s$	56
0.6	0.4	0	936076.20	110472.28	97154.53	$[1_221_32_31_32_212]_s$	52
0.8	0	0.2	940533.71	131692.21	98460.15	$[1_221_32_21_22_6]_s$	64
0.8	0.2	0	939987.74	121082.25	98005.70	$[121_221_4212_21_3]_s$	58
1	0	0	940647.25	131692.21	98559.41	$[1_32_21_32_31_5]_s$	64

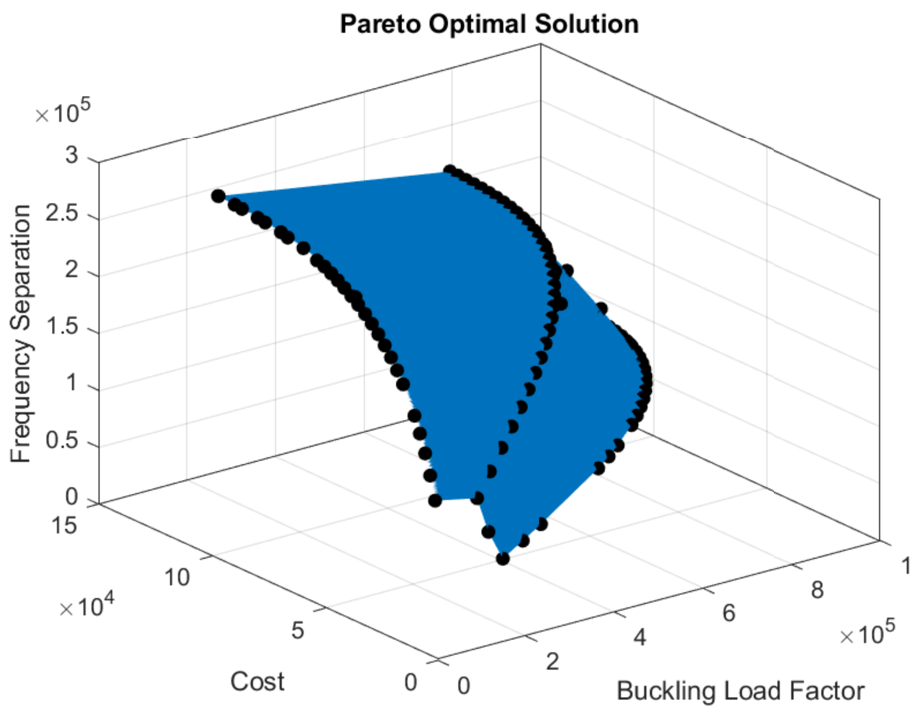

Figure 4.3 : Pareto optimal results for DC1a.

Table 4.7 : DC1b, weighted sum method.

Buckling load factor weight (w_1)	Cost weight (w_2)	Frequency sep. weight (w_3)	Buckling load factor	Cost	Frequency separation	Stacking Sequence	K_c
0	0	1	387870.30	131684.70	383560.75	$[31_2 3_2 1_2 313_2 1_2 3_2 1]_s$	64
0	0.2	0.8	387341.66	117538.89	380294.28	$[1_2 3_3 1_2 3_3 13_5]_s$	56
0	0.4	0.6	377299.08	92783.70	369847.92	$[13_3 1_2 31_3 312132]_s$	42
0	0.6	0.4	331503.97	64492.07	340194.69	$[31_3 3_4 1313_2 2_2 1]_s$	26
0	0.8	0.2	206556.79	32663.98	258728.82	$[13_2 13_2 1_2 313_2 13_2 2]_s$	8
0	1	0	136736.65	18518.16	150157.70	$[1_2 2_3 131_2 2_6 1]_s$	0
0.2	0	0.8	657739.33	131684.70	363838.70	$[2_{16}]_s$	64
0.2	0.2	0.6	656772.63	117538.89	360772.17	$[2_{16}]_s$	56
0.2	0.4	0.4	646728.04	99856.61	354697.34	$[2_{16}]_s$	46
0.2	0.6	0.2	624554.41	85710.80	346161.84	$[2_{16}]_s$	38
0.2	0.8	0	569648.99	68028.52	328095.79	$[2_{16}]_s$	28
0.4	0	0.6	657739.33	131684.70	363838.70	$[2_{16}]_s$	64
0.4	0.2	0.4	656772.63	117538.89	360772.17	$[2_{16}]_s$	56
0.4	0.4	0.2	650005.75	103393.07	356238.70	$[2_{16}]_s$	48
0.4	0.6	0	637635.03	92783.70	350954.64	$[2_{16}]_s$	42
0.6	0	0.4	657739.33	131684.70	363838.70	$[2_{16}]_s$	64
0.6	0.2	0.2	656772.63	117538.89	360772.17	$[2_{16}]_s$	56
0.6	0.4	0	652558.43	106929.52	357592.87	$[2_{16}]_s$	50
0.8	0	0.2	657739.33	131684.70	363838.70	$[2_{16}]_s$	64
0.8	0.2	0	656772.63	117538.89	360772.17	$[2_{16}]_s$	56
1	0	0	657739.33	131684.70	363838.70	$[2_{16}]_s$	64

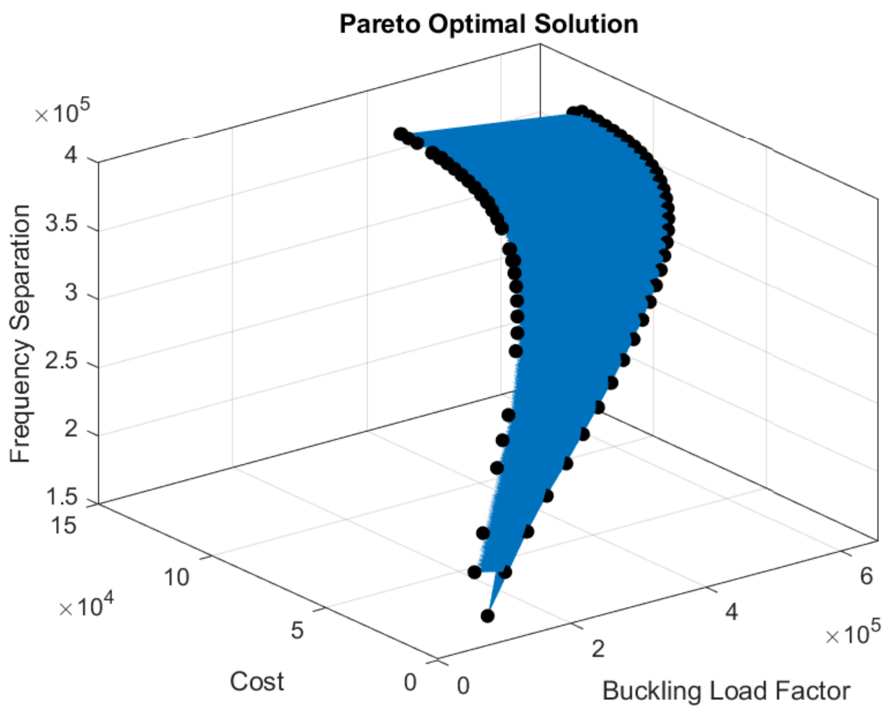

Figure 4.4 : Pareto optimal results for DC1b.

Table 4.4 and Table 4.6 consider plates with edge lengths that are exact opposites and subjected to the same loading conditions. It can be observed that as the buckling load factor weight increases, the laminates exhibit a stacking sequence that is the exact inverse. For instance, in the case where $w_1 = 1, w_2 = w_3 = 0$, Table 4.4 includes $\pm45^\circ_2$ and 90°_2 degree plies, while Table 4.6 utilizes 0°_2 and $\pm45^\circ_2$ degree plies. Additionally, the numerical values are quite close to each other. As the significance of the cost function increases, the number of carbon plies used decreases, which in turn reduces the critical buckling factor.

As shown in Table 4.7, the plate has transformed into a square shape, leading the $\pm45^\circ_2$ plies to produce the highest buckling load factor. For the cases of $w_1 = 1, w_2 = w_3 = 0$ and $w_3 = 1, w_1 = w_2 = 0$ the ply configurations result in approximately a 5% difference in frequency separation. The obtained cost values are consistent with Table 4.4 and Table 4.6.

4.2.4 Effect of load ratio

In order to observe the effect of the load ratio on the results, the design cases shown in Table 4.8 were examined. When determining the load ratios, the goal was to keep the total load magnitude constant. The aspect ratio was also kept constant.

Table 4.8 : Design cases DC2.

Design Case	Aspect Ratio	N_x [N/m]	N_y [N/m]	Load Ratio
DC2a	2	$\sqrt{2/5}$	$\sqrt{8/5}$	0.5
DC2b	2	$\sqrt{8/5}$	$\sqrt{2/5}$	2
DC2c	2	1	1	1

Table 4.9 and Figure 4.5 present the results for DC2a, while Table 4.10 and Figure 4.6 show the results for DC2b. The results for DC2c were previously shown in Table 4.4 and Figure 4.2.

Table 4.9 : DC2a, weighted sum method.

Buckling load factor weight (w_1)	Cost weight (w_2)	Frequency sep. weight (w_3)	Buckling load factor	Cost	Frequency separation	Stacking Sequence	K_c
0	0	1	155063.73	131692.21	268975.70	$[1_{11}2121_2]_s$	64
0	0.2	0.8	153219.65	110472.28	265225.35	$[1_{11}21321]_s$	52
0	0.4	0.6	143807.10	82179.03	253650.52	$[1_{10}2_212_23]_s$	36
0	0.6	0.4	126507.98	57422.44	228064.78	$[1_{16}]_s$	22
0	0.8	0.2	89379.26	25592.53	147764.01	$[1_{16}]_s$	4
0	1	0	122228.15	18519.22	104278.74	$[1_22_3131_22_61]_s$	0
0.2	0	0.8	615496.17	131692.21	235315.81	$[2_{16}]_s$	64
0.2	0.2	0.6	612498.36	110472.28	232013.85	$[2_{16}]_s$	52
0.2	0.4	0.4	601617.43	96325.65	228117.93	$[2_{16}]_s$	44
0.2	0.6	0.2	839410.80	85715.68	56847.95	$[3_62323_7]_s$	38
0.2	0.8	0	816093.17	78642.37	55591.19	$[3_423_523_5]_s$	34
0.4	0	0.6	816265.57	131692.21	105245.61	$[23_62_432_33]_s$	64
0.4	0.2	0.4	881124.52	114008.93	58992.13	$[3_62323_323_3]_s$	54
0.4	0.4	0.2	873547.10	103398.97	58253.83	$[3_623_2232_232_2]_s$	48
0.4	0.6	0	863593.65	96325.65	57663.73	$[3_7232_7]_s$	44
0.6	0	0.4	883806.53	131692.21	59528.59	$[3_323_{10}2_2]_s$	64
0.6	0.2	0.2	882433.34	117545.59	59087.60	$[3_72_2323_5]_s$	56
0.6	0.4	0	879451.60	110472.28	58653.27	$[3_7232_2323_3]_s$	52
0.8	0	0.2	883806.53	131692.21	59528.59	$[3_423_62323_3]_s$	64
0.8	0.2	0	882433.34	117545.59	59087.60	$[3_62323_323_3]_s$	56
1	0	0	883806.53	131692.21	59528.59	$[3_423_62323_2]_s$	64

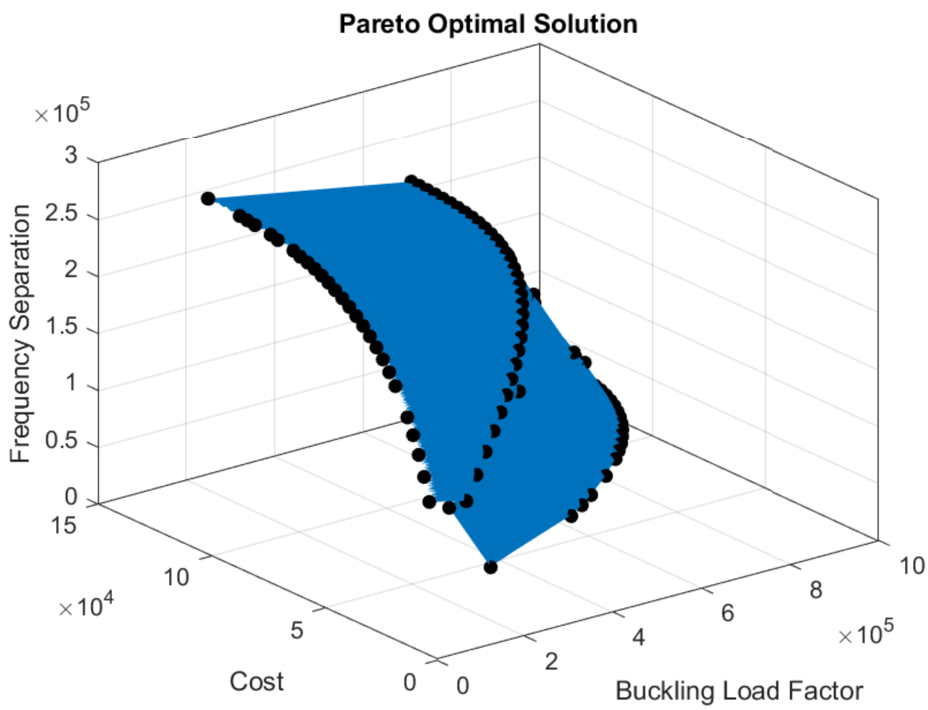

Figure 4.5 : Pareto optimal results for DC2a.

Table 4.10 : DC2b, weighted sum method.

Buckling load factor weight (w_1)	Cost weight (w_2)	Frequency sep. weight (w_3)	Buckling load factor	Cost	Frequency separation	Stacking Sequence	K_c
0	0	1	232595.59	131692.21	268975.70	$[1_{11}2121_2]_s$	64
0	0.2	0.8	229829.48	110472.28	265225.35	$[1_{11}21321]_s$	52
0	0.4	0.6	215710.64	82179.03	253650.52	$[1_{10}2_2 12_2 3]_s$	36
0	0.6	0.4	189761.97	57422.44	228064.78	$[1_{16}]_s$	22
0	0.8	0.2	134068.88	25592.53	147764.01	$[1_{16}]_s$	4
0	1	0	183342.23	18519.22	104278.74	$[1_2 2_3 131_2 2_6 1]_s$	0
0.2	0	0.8	923244.26	131692.21	235315.81	$[2_{16}]_s$	64
0.2	0.2	0.6	920642.00	114008.93	232707.92	$[2_{16}]_s$	54
0.2	0.4	0.4	1110209.41	99862.31	143475.96	$[2_2 323_3 232323_4]_s$	46
0.2	0.6	0.2	1095040.77	92789.00	141846.08	$[32_2 3_2 2_4 3_7]_s$	42
0.2	0.8	0	1058883.07	82179.03	138637.85	$[3_2 2_3 32_3 3_3 2_4]_s$	36
0.4	0	0.6	1129203.41	131692.21	147067.93	$[3_2 2_3 32_2 32_7]_s$	64
0.4	0.2	0.4	1127588.47	117545.59	145815.75	$[2323_2 232_4 323_3]_s$	56
0.4	0.4	0.2	1120465.32	106935.62	144507.00	$[3_2 2_2 32_6 3_3 23]_s$	50
0.4	0.6	0	1116061.46	103398.97	143990.79	$[232_2 3_3 2_2 323_5]_s$	48
0.6	0	0.4	1129203.41	131692.21	147067.93	$[2_2 323_3 2_2 3_3 23_3]_s$	64
0.6	0.2	0.2	1127477.26	117545.59	145863.77	$[3_2 2_2 32_6 3_2 23_2]_s$	56
0.6	0.4	0	1126043.54	114008.93	145420.57	$[32_2 3_2 2_3 3232_5]_s$	54
0.8	0	0.2	1129203.41	131692.21	147067.93	$[2323232_2 3_2 23_5]_s$	64
0.8	0.2	0	1127588.47	117545.59	145815.75	$[2_2 3_2 23_2 23_2 32_2 3_2]_s$	56
1	0	0	1129190.39	131692.21	147019.58	$[23_2 232_2 32_3 32_4]_s$	64

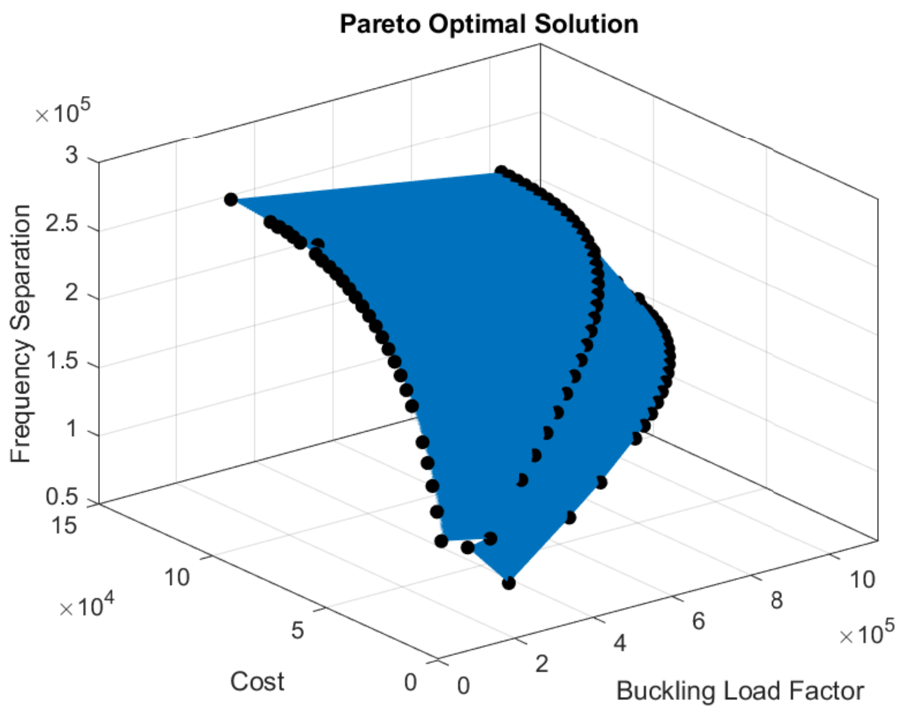

Figure 4.6 : Pareto optimal results for DC2b.

When evaluating the results in Table 4.4, Table 4.9, and Table 4.10, it can be said that the maximum critical buckling factor is inversely proportional to the Nx/Ny ratio. Due to the aspect ratio, where the length of side a is twice that of side b, the increased proportion of the N_y load results in a greater load being applied to the plate and consequently reduces the critical buckling load. Also, it is observed that these three cases have exhibited similar trends in laminate stacking sequence.

5. CONCLUSIONS

This thesis focused on the multi-objective optimization of a layered hybrid (carbon/epoxy and glass/epoxy) composite plate consisting of 64 plies. Utilizing the particle swarm optimization algorithm, the objectives were to maximize the critical buckling load and the difference between the first two natural frequency values, while minimizing the cost function. Ply material and ply orientation were selected as design variables.

In the first section of the study, two objective functions were selected, and the algorithm was repeatedly executed for these functions. According to the obtained results, numerous points that both maximized the buckling load and minimized the cost were identified in the solution space. Two different methods were used to show that these points form a curve.

In the second part, all objective functions were included in the calculations, and the analyses were repeated. This time, the obtained points corresponded to a surface rather than a curve. While the majority of points were located on three different curves, some were positioned on the surface. Hence, it can be concluded that any point on the surface constitutes an element of the optimal solution.

Subsequently, the analysis was repeated for different aspect ratios and load ratios. The analysis included three different scenarios with varied a and b values to evaluate the impact of aspect ratio. By keeping the plate area constant, which is directly linked to cost, it was observed that the a/b ratio directly influences the orientation of plies.

Lastly, with an aspect ratio of 2, changes in the load ratio were examined to assess its impact. For a more accurate evaluation, efforts were made to maintain consistent magnitudes of the loads acting on the plate. With an aspect ratio of 2, the increase in the N_x/N_y ratio leads to a greater total load on the plate and consequently decreases the critical buckling load. When determining the critical buckling load of a plate, it is necessary to consider both the aspect ratio and the load ratio as two parameters that should be evaluated together.

REFERENCES

[1] **Karakaya, S. and Soykasap, O.** (2011). Natural frequency and buckling optimization of laminated hybrid composite plates using genetic algorithm and simulated annealing., *Structural and Multidisciplinary Optimization*, *43*, 61–72.

[2] **Pal, S.**, **Kalita, K.**, **Majumdar, A. and Haldar, S.** (2023). Optimization of frequency separation of laminated shells carrying transversely distributed mass using genetic algorithm, *Journal of Vibration and Control*, 10775463231190277.

[3] **Ashwear, N.**, **Tamadapu, G. and Eriksson, A.** (2016). Optimization of modular tensegrity structures for high stiffness and frequency separation requirements, *International Journal of Solids and Structures*, *80*, 297–309.

[4] **Nettles, A.T.** (1994). Basic mechanics of laminated composite plates, **Technical Report**.

[5] **Berthelot, J.M.** (1999). Composite materials: mechanical behavior and structural analysis, *(No Title)*.

[6] **Öchsner, A.** (2023). *Composite mechanics*, volume184, Springer Nature.

[7] **Jones, R.M.** (2018). *Mechanics of composite materials*, CRC press.

[8] **Leissa, A.W.** (1985). *Buckling of laminated composite plates and shell panels*, Flight Dynamics Laboratory.

[9] **Duffy, K. and Adali, S.** (1990). Design of antisymmetric hybrid laminates for maximum buckling load: II. Optimal layer thickness., *Composite Structures*, *14*(2), 113–124.

[10] **Riche, R.L. and Haftka, R.** (1995). Improved genetic algorithm for minimum thickness composite laminate design., *Composites Engineering*, *5*(2), 143–161.

[11] **Haftka, R.**, **Kogiso, N.**, **Watson, L. and Gürdal, Z.** (1994). Genetic algorithms with local improvement for composite laminate design., *Structal Optimization*, *7*, 207–218.

[12] **Eberhart, R. and Kennedy, J.** (1995). A new optimizer using particle swarm theory., *MHS'95. Proceedings of the Sixth International Symposium on Micro Machine and Human Science.*, 39–43.

[13] **Eberhart, R. and Shi, Y.** (2000). Comparing inertia weights and constriction factors in particle swarm optimization., *Proceedings of the 2000 Congress on Evolutionary Computation. CEC00 (Cat. No.00TH8512)*, *1*, 84–88.

[14] **Adali, S. and Verijenko, V.** (2001). Optimum stacking sequence design of symmetric hybrid laminates undergoing free vibrations, *Composite Structures*, *54*(2), 131–138, `https://www.sciencedirect.com/science/article/pii/S0263822301000800`, third International Conference on Composite Science and Technology.

[15] **Li, M.**, **Guedes Soares, C.**, **Liu, Z. and Zhang, P.** (2024). Free and Forced Vibration Analysis of Carbon/Glass Hybrid Composite Laminated Plates Under Arbitrary Boundary Conditions, *Applied Composite Materials*, 1–24.

[16] **Spallino, R. and Rizzo, S.** (2002). Multi-objective discrete optimization of laminated structures., *Mechanics Research Communications*, *1*(29), 17–25.

[17] **Suresh, S.**, **Sujit, P. and Rao, A.** (2007). Particle swarm optimization approach for multi-objective composite box-beam design, *Composite Structures*, *81*(4), 598–605.

[18] **Abachizadeh, M. and Tahani, M.** (2009). An ant colony optimization approach to multi-objective optimal design of symmetric hybrid laminates for maximum fundamental frequency and minimum cost., *Struct Multidisc Optim*, *37*, 367–376.

[19] **Yıldız, K. and Lesieutre, G.A.** (2020). Sizing and prestress optimization of Class-2 tensegrity structures for space boom applications., *Engineering with Computers*, *38*(2), 1451–1464.

[20] **Konak, A.**, **Coit, D. and Smith, A.** (2006). Multi-objective optimization using genetic algorithms: A tutorial., *Reliability Engineering and System Safety*, *91*, 992–1007.

[21] **Serhat, G. and Basdogan, I.** (2019). Multi-objective optimization of composite plates using lamination parameters, *Materials Design*, *180*, 107904, `https://www.sciencedirect.com/science/article/pii/S0264127519303429`.

[22] **Kassapoglou, C.** (2013). *Design and analysis of composite structures: with applications to aerospace structures*, John Wiley & Sons.

[23] **Reddy, J.N.** (2003). *Mechanics of laminated composite plates and shells: theory and analysis*, CRC press.

[24] **Barbero, E.J.** (2010). *Introduction to composite materials design*, CRC press.

[25] **Gürdal, Z.**, **Haftka, R.T. and Hajela, P.** (1999). *Design and optimization of laminated composite materials*, John Wiley & Sons.

[26] **Vanderplaats, G.N.**, (1987). Numerical optimization techniques, Computer aided optimal design: structural and mechanical Systems, Springer, pp.197–239.

APPENDICES

APPENDIX A : Optimization Results

APPENDIX A : Optimization Results

All optimization results obtained for the 3 objective functions can be accessed in the link below:

- `https://kovan.itu.edu.tr/index.php/s/YKKgSTYz4kTSBGw`

CURRICULUM VITAE

Name SURNAME: Orhan Nuri YEGIT

EDUCATION:

- **B.Sc.:** 2020, Istanbul Technical University, Faculty of Aeronautics and Astronautics, Aeronautical Engineering

PROFESSIONAL EXPERIENCE AND REWARDS:

- 2020-present, Turkish Aerospace Industry - Structural Analysis Engineer

PUBLICATIONS, PRESENTATIONS AND PATENTS ON THE THESIS:

- **Yegit O. N.**, Yildiz K. (2024). Fiber Takviyeli Katmanlı Hibrit Kompozit Plakaların Parçacık Sürü Algoritması ile Çok Amaçlı Optimizsyonu. *ULUSAL HAVACILIK VE UZAY KONFERANSI*, September 18-20, 2024 Ankara, Turkey.